

AFWL-TR-74-338

AFWL-TR-74-338

FG

12

ADA022260



# SELF-CONSISTENCY AND RADIATION ENHANCED GROUND CONDUCTIVITY IN THE SURFACE BURST CODE SCX

Science Applications Corporation  
La Jolla, CA 92037

November 1975

Final Report

Approved for public release; distribution unlimited.

This research was sponsored by the Defense Nuclear Agency under Subtask R99QAXEA094, Work Unit 41, Work Unit Title: Low Altitude Predictions.

Prepared for  
Director  
DEFENSE NUCLEAR AGENCY  
Washington, DC 20305

AIR FORCE WEAPONS LABORATORY  
Air Force Systems Command  
Kirtland Air Force Base, NM 87117

DDC  
RECEIVED  
MAR 26 1976  
REGISTRY  
C




388862

AFWL-TR-74-338

This final report was prepared by the Science Applications Corporation, LaJolla, California under Contract F29601-74-C-0006, Job Order WDNE0707 with the Air Force Weapons Laboratory, Kirtland Air Force Base, New Mexico. Capt. William A. Seidler (ELP) was the Laboratory Project Officer-in-Charge.

When US Government drawings, specifications, or other data are used for any purpose other than a definitely related Government procurement operation, the Government thereby incurs no responsibility nor any obligation whatsoever, and the fact that the Government may have formulated, furnished, or in any way supplied the said drawings, specifications, or other data is not to be regarded by implication or otherwise as in any manner licensing the holder or any other person or corporation or conveying any rights or permission to manufacture, use, or sell any patented invention that may in any way be related thereto.

This technical report has been reviewed and is approved for publication.



WILLIAM A. SEIDLER  
Capt, USAF  
Project Officer

FOR THE COMMANDER




LARRY W. WOOD  
LtCol, USAF  
Chief, Phenomenology and  
Technology Branch



JOHN W. SWAN  
Colonel, USAF  
Chief, Electronics Division

This report has been reviewed by the Information Office (OI) and is releasable to the National Technical Information Service (NTIS). At NTIS, it will be available to the general public, including foreign nations.

ACCESSION for	White Section	<input type="checkbox"/>
NTIS	Def Section	<input type="checkbox"/>
DDC		
UNASSIGNED		
JUSTIFICATION		
BY	DISTRIBUTION AVAILABILITY CODES	
	MAIL ROOM/ST 5	



DO NOT RETURN THIS COPY. RETAIN OR DESTROY.

UNCLASSIFIED

SECURITY CLASSIFICATION OF THIS PAGE (When Data Entered)

18 (19) REPORT DOCUMENTATION PAGE		READ INSTRUCTIONS BEFORE COMPLETING FORM
1. REPORT NUMBER AFWL-TR-74-338	2. GOVT ACCESSION NO.	3. RECIPIENT'S CATALOG NUMBER
4. TITLE (and Subtitle) SELF-CONSISTENCY AND RADIATION ENHANCED GROUND CONDUCTIVITY IN THE SURFACE BURST CODE SCX.	5. TYPE OF REPORT & PERIOD COVERED Final Report.	
7. AUTHOR(s) B. H. Fishbine, S. J. Dalich & J. N. Wood	6. PERFORMING ORG. REPORT NUMBER SAI-74-505-AQ	8. CONTRACT OR GRANT NUMBER(s) F29601-74-C-0006 NEW
9. PERFORMING ORGANIZATION NAME AND ADDRESS Science Applications Corp. 1200 Prospect Street, P.O. Box 2351 LaJolla, CA. 92037	10. PROGRAM ELEMENT, PROJECT, TASK AREA & WORK UNIT NUMBERS 62707H, WDNE-070Z Subtask: R99QAXEA094 Work Unit: 41	
11. CONTROLLING OFFICE NAME AND ADDRESS Director Defense Nuclear Agency Washington, DC 20305	12. REPORT DATE November 1975	13. NUMBER OF PAGES 54
14. MONITORING AGENCY NAME & ADDRESS (if different from Controlling Office) Air Force Weapons Laboratory Air Force Systems Command Kirtland AFB, NM 87117	15. SECURITY CLASS. (of this report) Unclassified	15a. DECLASSIFICATION/DOWNGRADING SCHEDULE
16. DISTRIBUTION STATEMENT (of this Report) Approved for public release; distribution unlimited. 17 A094 16 DNA-NWET-QAXE		
17. DISTRIBUTION STATEMENT (of the abstract entered in Block 20, if different from Report)		
18. SUPPLEMENTARY NOTES This research was sponsored by the Defense Nuclear Agency under Subtask R99QAXEA094, Work Unit 41, Work Unit Title Low Altitude Predictions.		
19. KEY WORDS (Continue on reverse side if necessary and identify by block number) Electromagnetic Pulse (EMP) High Altitude EMP EMP Code Development EMP Prediction Techniques		
20. ABSTRACT (Continue on reverse side if necessary and identify by block number) A description of the numerical techniques used to include the self-consistent effect in the two-dimensional ground burst EMP code, SCX, is given. The effect of this phenomenon on the fields predicted by SCX is discussed and illustrated. The effect is most notable for observer positions less than 2,000 meters from the burst point where a sign change occurs in the transverse E field.		

NEXT PAGE

Handwritten marks and signature at the bottom right of the page.

UNCLASSIFIED

SECURITY CLASSIFICATION OF THIS PAGE(When Data Entered)

△ Also presented are discussion and results concerning the inclusion of a radiation enhanced ground conductivity model in SCX. Results of calculations with this model indicate that for a zero height of burst situation, field effects are minimal. △

UNCLASSIFIED

SECURITY CLASSIFICATION OF THIS PAGE(When Data Entered)

## TABLE OF CONTENTS

	<u>Page</u>
SECTION I - INTRODUCTION	1
SECTION II - A DESCRIPTION OF THE SELF-CONSISTENCY MODEL	3
SECTION III - THE EFFECT OF SELF-CONSISTENCY ON THE CURRENTS	12
SECTION IV - THE EFFECT OF SELF-CONSISTENCY ON THE FIELDS	16
SECTION V - RADIATION ENHANCED GROUND CONDUCTIVITY	32
REFERENCES	37

## LIST OF FIGURES

<u>Figure</u>		<u>Page</u>
1	The field space used in the interpolation scheme.	7
2	Scaling self-consistent currents by the time-step factor.	11
3	Overlay of non-self-consistent and self-consistent radial currents at 500m, on the ground.	20
4	Overlay, theta currents, 500m.	20
5	Self-consistent theta current at 500m, on the ground.	21
6	Overlay, conductivities, 500m.	21
7	Overlay, radial electric fields, 500m.	22
8	Non-self-consistent theta electric field at 500m, on the ground.	22
9	Self-consistent theta electric field at 500m, on the ground.	23
10	Overlay, theta electric fields, 500m.	23
11	Overlay, axial magnetic field, 500m.	24
12	Overlay, radial currents, 1000m.	24
13	Overlay, theta currents, 1000m.	25
14	Self-consistent theta current at 1000m, on the ground.	25
15	Overlay, conductivities, 1000m.	26
16	Overlay, radial electric fields, 1000m.	26
17	Non-self-consistent theta electric field at 1000m, on the ground.	27
18	Self-consistent theta electric field at 1000m, on the ground.	27

LIST OF FIGURES (Continued)

<u>Figure</u>		<u>Page</u>
19	Overlay, theta electric fields, 1000m.	28
20	Overlay, axial magnetic field, 1000m.	28
21	Overlay, radial currents, 2000m.	29
22	Overlay, theta currents, 2000m.	29
23	Overlay, conductivity, 2000m.	30
24	Overlay, radial electric fields, 2000m.	30
25	Overlay, theta electric fields, 2000m.	31
26	Overlay, axial magnetic fields, 2000m.	31
27	Radiation Enhanced Ground Conductivity vs. Time for Range of 250m and Depth of .05m.	36

2

SECTION I  
INTRODUCTION

SCX is a two dimensional ground burst EMP (electromagnetic pulse) computer code. The general numerical methods used in the code are documented<sup>(1)</sup> elsewhere and will not be discussed here. Briefly, the code obtains the solution to Maxwell's equations in the source region of a surface nuclear burst. Because the solution is obtained in the source region, several nonlinearities are inherent to the problem. First, the conductivity of the medium depends strongly on the total electric field. The effect has always been modeled in the code. Second, the source terms are themselves influenced by the fields. This effect is generally referred to as "self-consistency", and until recently was not included in the SCX code. This paper reviews the methods used to model self-consistency in SCX, and presents comparative results of calculations before and after the effect was included in SCX.

An exact representation of self-consistency requires the solution to the equations of motion for the Compton electrons. Clearly, for an EMP computer code with two space dimensions plus time, this is impractical. The amount of storage required is not available, and the running time would render the code economically useless. Fortunately, methods have been devised which allow for the inclusion of the self-consistent effect in an approximate fashion<sup>(2)</sup>. These methods require a minimal amount of storage and cause only slight increases in running time.

The sources of the EMP are the Compton recoil electrons created through the device radiation interactions with the atmosphere. In SCX these sources are described as current densities in the radial and transverse directions. The current densities were obtained from Monte Carlo transport calculation results which were then curve fit for use in the code. The transport results, being completely independent of the EMP calculation, do not contain any effects due to interactions with



electromagnetic fields. To include the self-consistent effect, some modification must be made to the source terms within the SCX code. This leads to several necessary approximations, the impact of which will be discussed below.

SECTION II  
A DESCRIPTION OF THE SELF-CONSISTENCY MODEL

The self-consistency model used is derived from EMP Theoretical Note 77, Volume 2-4, by H. J. Longley.<sup>(2)</sup> The note describes a way of modifying a purely radial, analytic current source to obtain self-consistent radial and transverse currents. The method is based on electron turning in the presence of electromagnetic fields.

To determine the amount of turning, a group of electrons is followed in various time constant electromagnetic environments. These electrons are recoils created by Compton scattered, monoenergetic gamma rays and are chosen to represent a physically realistic distribution of Compton recoil angles and energies. The equations of motion for the electrons are differenced and solved numerically. The computation proceeds in time until an electron's kinetic energy is within 1% of its rest mass energy. In STP air, 1 MeV electron has a range of .49 g/cm<sup>2</sup>. An electron with a kinetic energy equal to 10% of its rest mass energy, has a range of .0049 g/cm<sup>2</sup>. So a 1 MeV electron slowed to 1% of its rest mass energy is easily within 1% of its final range. At this point, the electron's final radial and transverse positions are recorded. An average is taken of the final positions for the group of electrons and these averages are used to obtain self-consistent currents. The validity of this method depends on the lifetimes of the electrons and the time steps used in the SCX calculation. This matter will be discussed later.

To obtain the self-consistent radial current, the original radial, analytic current is multiplied by  $DX/R_{mf}$  where  $DX$  is the average electron final radial position and  $R_{mf}$  is the mean forward range of the electron in the absence of fields. The self-consistent transverse current is obtained by multiplying the original radial current by  $DY/R_{mf}$ , where  $DY$  is the average electron final transverse position. In the earth's magnetic field, the Larmor radius of a 1 MeV electron is about 100 times

its range. Since typical EMP fields produce much greater effects, such as reversing the transverse current obtained from Monte Carlo transport calculations, the geomagnetic field will be neglected.

Two items are important in this method. The first is the initial kinetic energy,  $E_e$ , of an electron to be tracked. This energy depends on the initial gamma energy,  $E_{\gamma 0}$ , and the scattering angle and is obtained directly from the Klein-Nishina equation. The second item of importance is the calculation of  $R_{mf}$ .  $R_{mf}$  is the mean forward range obtained by

$$R_{mf} = \frac{1}{\sigma_c} \int_{\theta_e = 0}^{\pi/2} R \cos \theta_e \sigma_e d\Omega_e \quad (1)$$

where

$$\sigma_c = \int_{\theta_e = 0}^{\pi/2} \sigma_e d\Omega_e \quad (2)$$

and  $\sigma_e$  is the angular differential cross-section obtained from the Klein-Nishina formula,  $d\Omega_e$  is the solid angle associated with the scattering angle  $\theta_e$  of the recoil electron,  $\theta_e$  is the angle between the initial direction of propagation of the gamma and the direction of the electron's recoil.  $R$  is the range obtained from a fit to experimental mean range versus energy data. The energy used to obtain  $R$  is  $E_e$  which is a function of  $E_{\gamma 0}$  and  $\theta_e$ .

Our method of obtaining self-consistent currents is different in several respects from the method described in EMP Theoretical Note 77. Where Longley's method used only an analytic, radial current source; the current sources used in SCX have both radial and transverse components. The general method described in Note 77 is designed for use with an analytic current source. The source terms in SCX are, however, not analytic, having been obtained through curve fits to the results of gamma and neutron Monte Carlo transport calculations. The source terms serve as inputs to SCX, and are expressed

as total currents in the radial and transverse directions. In order to adapt the general method to our purposes, tables similar to Longley's were generated. However, our tables are for electrons recoiling in the same direction as the initial gamma propagation direction and are not averages of electrons recoiling at different  $\theta_e$ . This was done because the transport calculations which provide the current sources for SCX already include angular scatter effects and the electron energy spectrum is already folded in.

In applying DX/R and DY/R factors to the SCX transport derived currents, first a total initial current is calculated from the initial transport derived radial and transverse currents. This total current is then treated in the same manner that the analytic radial current source is treated in Longley's method. To accomplish this, the angle between the positive radial axis and the total initial current is used to transform the radial and transverse electric fields to a new primed coordinate system where the total initial current is parallel to the primed positive radial axis (i.e., a transformation to a coordinate system in which the transverse current is zero). The DX/R and DY/R factors are applied to the total initial current and the resulting primed self-consistent radial and transverse currents are transformed back to the original coordinate system to obtain the final self-consistent currents.

In addition to following single electrons rather than probabilistically representative groups, our method differs from Longley's in two respects. First, rather than using the initial electron kinetic energy calculated directly from the Klein-Nishina equation, a mean initial electron energy is used. This energy is calculated by

$$\bar{E}_e = \frac{1}{\sigma_c} \int_{\theta_e=0}^{\pi/2} E_e \sigma_e d\Omega_e$$

Where  $E_e$  is a function of  $\theta_e$  and initial gamma energy,  $E_{\gamma_0}$ , and is calculated from the Klein-Nishina equation.

Secondly, the range we use is different from  $R_{mf}$ , the mean forward range used by Longley. We use a range  $R_c$ , which is the electron range calculated by the electron tracking subroutine with all fields set to zero. This range differs from the range obtained by using  $\bar{E}_e$  and the  $R$  in Eqn. (1) only because of roundoff error.

In Longley's scheme, tables of  $DX$  and  $DY$  were generated for various field values and gamma energies. These tables were then fit by analytic functions and the functions used to introduce self-consistency into the LEMP code. In our case, tables of  $DX/R_c$  and  $DY/R_c$  are generated and used directly by SCX, along with some interpolation coding, to obtain self-consistency. The interpolation scheme is simple-minded and chosen to supply smooth sources to SCX.

The interpolation is basically as follows. The three field values calculated by SCX are the radial electric field ( $E_r$ ), the transverse electric field ( $E_\theta$ ) and the phi magnetic field ( $B_\phi$ ). These fields can be thought of as the three coordinates of a field space. For the  $DX/R_c$  tables each entry in the table represents a point in the field space. Similarly for  $DY/R_c$ . For a given set of field values calculated by SCX, the interpolation coding determines what eight points, the vertices of a rectangular solid, corresponding to given  $DX/R_c$  or  $DY/R_c$  surround the point  $P$  whose coordinates are given by the three field values. This rectangular solid can be broken up into eight sub-solids by passing three planes through the fields value point. The planes are parallel to the six faces of the original solid and generate one sub-solid for each vertex of the original solid. The interpolation scheme weights the  $DX/R_c$  or  $DY/R_c$  value at a particular vertex by a volume obtained by subtracting the volume of the sub-solid of that vertex from the volume of the original solid. This weighting is done for all eight points, summed and divided by the total volume of the original solid. The scheme is smooth and has the advantage

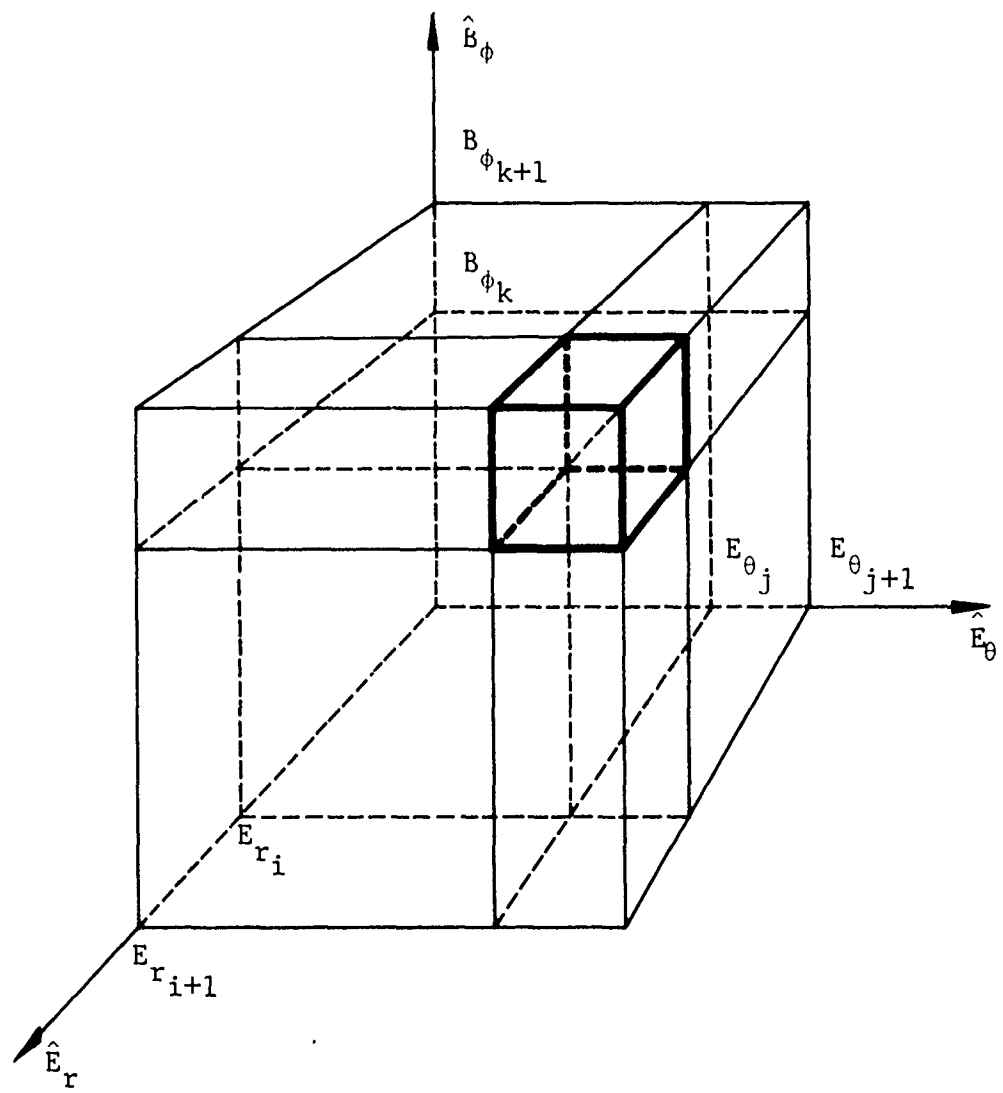


Fig. 1. The field space used in the interpolation scheme.

that if the fields values fall exactly on a point in the tables, the precise values of  $DX/R_c$  and  $DY/R_c$  from the tables are obtained.

The equation of motion used in the electron tracker subroutine is:

$$\dot{\vec{p}} = -|e| \left\{ \vec{E} + \dot{\vec{v}} \times \vec{B} \right\} - A \frac{\dot{\vec{p}}}{|\dot{\vec{p}}|}$$

where  $\dot{\vec{p}}$  is the electron's momentum,  $e$  the electron's charge,  $\dot{\vec{v}}$  the electron's velocity,  $\vec{E}$  the electrical intensity of the environment,  $\vec{B}$  the magnetic intensity, and  $A$  is a slowing term like  $\frac{dE}{ds}$  which includes energy losses due to ionization, multiple scattering and radiation. If  $\vec{E}$  and/or  $\vec{B}$  are large enough their contributions will overcome the energy loss term  $A$  and the electrons will never come to rest. These are termed run-away electrons. The self-consistency model used here includes a range of field values which generate  $DX/R_c$  and  $DY/R_c$  tables that exclude run-away electrons. Therefore, the interpolation coding holds field values to the limits used in generating the tables.

In estimating the effect of self-consistency on the conductivity we have to consider the effects of the electric fields on an electron's kinetic energy, since the kinetic energy determines the amount of ionization. If an electron has an initial velocity in a given direction an electric field parallel to the velocity vector will increase or decrease the electron's kinetic energy depending on the sign of the field.

Generally, the direction of the radial electric field is positive, away from the burst source point. Similarly for the Compton recoil electrons. Therefore, the radial electric field tends to reduce the recoil electron energy and thereby reduce the ionization due to electrons. Initially the theta electron velocity in the transformed system is zero so that the theta electric field will increase the electron's theta momentum

regardless of the field's sign. These approximate arguments lead to the following correction factor,  $f_q$ , to the ionization rate.

$$f_q = \frac{\bar{E}_e + W}{\bar{E}_e}$$

where

$$W = |e| \left\{ |E_\theta DY| - E_r DX \right\}$$

and  $|e|$  is the absolute value of the electron's charge.  $W$  is an estimate of the work done by the fields on the electron and therefore changes the energy available for ionization.

The applicability of this self-consistent scheme is questionable when the time steps used by fields code differencing are comparable or less than the lifetimes of the electrons. In real time, for gammas of 1.5 MeV, electron lifetimes are on the order of  $10^{-8}$  second. In retarded time, due to turning, this time may be much larger since there is a component of the electron velocity which is parallel to the gamma wave front.

In a typical SCX run, the time steps during the prompt gamma peak are  $10^{-9}$  second. After the peak, time steps are  $10^{-8}$  second and larger. By examining electron trajectories for typical SCX environments it is apparent that the electrons frequently turn back and complete loops. But it is still likely that the final position of an electron is in the same general direction from the electron's original position as the position of an electron at the end of a time step shorter than the electron's lifetime. Since the electron is slowing down, we expect that the electric fields, at least, will have more effect on the electron's position near the end of its life than at the beginning where it has large kinetic energy. In the present SCX calculations, the self-consistent effect is probably exaggerated during the prompt gamma peak.



An approximate correction in such situations might be to scale the turning by a factor  $t_s/t_{el}$ , where  $t_s$  is the time step and  $t_{el}$  is the electron lifetime. A better factor would be

$$f_t = (t_s/t_{el})^2$$

which more heavily weights time steps close to  $t_{el}$ . The  $f_t$  factor is plausible because the non-relativistic equation for a displacement  $s$  due to a constant force on a mass  $m$  is

$$s = \frac{F}{2m} t^2 .$$

The  $f_t$  factor would scale the angle that the position vector of the electron's final position makes with the initial gamma propagation direction. To accomplish this, take the original  $DX/R_c$  and  $DY/R_c$ . Compute

$$\alpha = \left\{ [DY/R_c] / [DX/R_c] \right\} = \tan \delta$$

$$m = \left\{ [DX/R_c]^2 + [DY/R_c]^2 \right\}^{1/2}$$

$$\beta = \arctan \left\{ \alpha \cdot f_t \right\}$$

$$[DX/R_c]' = m \cos (\beta)$$

$$[DY/R_c]' = m \sin (\beta)$$

and use  $[DX/R_c]'$  and  $[DY/R_c]'$  as before.

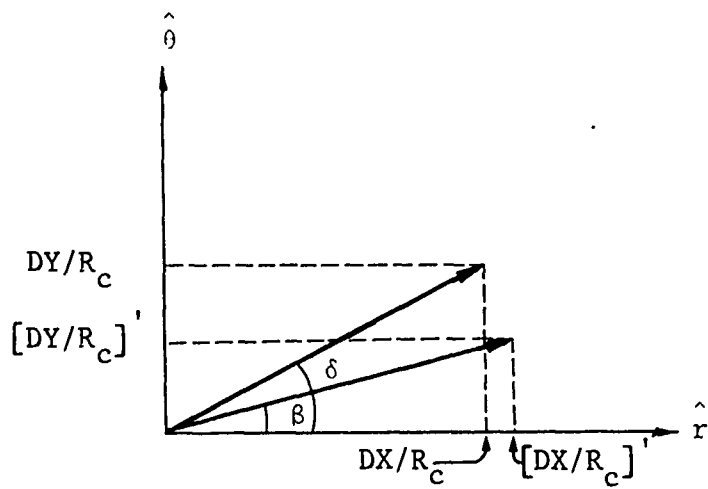


Fig. 2. Scaling Self-Consistent Currents by the Time-Step Factor.

SECTION III  
THE EFFECT OF SELF-CONSISTENCY ON THE CURRENTS

To interpret the plots overlaying self-consistent and non-self-consistent time histories of SCX runs, it is useful to first describe the individual effects of the fields on a single electron.

For an electric field  $\vec{E}$ , the force on a charge  $q$  is  $\vec{F} = \vec{E} q$ . An electron in a positive  $E_r$  field experiences a force in the  $-\hat{r}$  direction which contributes to a positive radial conventional current. Since the Compton recoil electrons are streaming radially outward, constituting a negative conventional current, the isolated effect of a positive  $E_r$  field is to reduce the magnitude of the negative radial current  $-J_r$ . The same type of argument indicates the effect of  $E_\theta$  on the theta current.

SCX calculates a  $B_\phi$  which is negative. Since  $|J_r|$  is usually greater than  $|J_\theta|$ , we first consider the effect of a magnetic field on a purely radial current.

An electron with a velocity  $\vec{v}$  in the  $+\hat{r}$  direction will experience a magnetic force  $\vec{F} = q(\vec{v} \times \vec{b})$ . For  $B_\phi$  negative  $\vec{F}$  will be in the  $-\hat{\theta}$  direction and so contribute to a positive theta conventional current.

Occasionally,  $J_r$  and  $J_\theta$  are the same order of magnitude. In the extreme case where the conventional current is purely in the  $-\hat{e}$  direction, the magnetic field will contribute to a negative radial conventional current.

In determining whether it is an electric field or the magnetic field which dominates the electron turning, it is useful to be able to make rough comparisons between the effects of the electric and magnetic fields.

For an electron of initial energy  $\bar{E}_e$ , initial speed  $v_0$ , and absolute charge  $e$ , we define  $F_m$  to be the maximum magnetic force on the electron and  $F_s$  to be the maximum slowing force on the

electron. Since these two forces are monotonically increasing functions of the electron velocity, (except for  $F_s$  when the electron energy is below 0.5 MeV) the maxima occur at the electron's maximum speed, i.e.,  $v_o$ . For an incident gamma of 1.5 MeV,  $E_e$  is .75 MeV and  $v_o$  is  $2.75 \times 10^8$  m/sec.  $F_m$  and  $F_s$  can then be compared as follows:

$$F_m/e = B_\phi \cdot 2.75 \times 10^8$$

$$F_s/e = \frac{A(v_o)}{e} = 3.49 \times 10^5$$

The slowing term  $A(v_o)$  is obtained from a fit to experimental data of electron energy as a function of electron mean range. This fit is differentiated with respect to range to obtain  $\frac{dE}{ds}$ .

With the use of  $F_m$  and  $F_s$  we can predict the combination of effects of the various fields on the currents.

The radial current overlays in Figs. 3 and 12 show that for ranges of 500m and 1000m the self-consistent model reduces the magnitude of the radial current until past a microsecond. This is especially noticeable at the time of the prompt gamma peak and also past 10 shakes where the reduction in  $J_r$  increases markedly with time until near a microsecond. The 2000m radial currents overlay exactly, which prompts us to consider the close-in ranges and the 2000m range separately. Evidently, at 2000m for this yield, the fields are reduced enough to show only small self-consistent effects, primarily in  $J_\theta$  and  $E_\theta$ .

As mentioned earlier, the effect of a positive  $E_r$  field is to reduce the magnitude of a negative  $J_r$ . For the two close-in ranges,  $E_r$  is positive throughout the calculation. Also, a negative  $B_\phi$  will only increase the magnitude of negative  $J_r$  when  $J_\theta$  is negative and  $|J_\theta| \sim |J_r|$ . In the self-consistent case, we see that  $|J_r|/|J_\theta|$  is close to unity at 1.4 usec. At this point, in Fig. 3, the self-consistent  $J_r$  is increased as expected. By comparing the

non-self-consistent  $J_\theta$  and  $J_r$ , it is seen that separation between the self-consistent  $J_r$  and non-self-consistent  $J_r$  continues to increase.

The more pronounced  $-J_r$  reduction at the time of the prompt gamma peak is due to the combined peaking of  $E_r$  and  $B_\phi$ . After the prompt gamma pulse, whereas  $E_r$  is saturated and remains reasonably constant out to neutron arrival at around 10 microseconds,  $B_\phi$  steadily increases in magnitude and thus increases the separation of the  $J_r$  overlays. It is interesting to note that at 500m the self-consistent  $B_\phi$  starts leveling off at around 2  $\mu$ sec and then starts to decrease at about 5  $\mu$ sec. The separation in the  $J_r$  overlays follows this behavior until the non-self-consistent  $J_\theta$  becomes larger than the non-self-consistent  $J_r$ . Similar behavior is shown at 1000m.

At 2000m there is no visible effect of the self-consistent model on the radial current. This is plausible on the basis of rough field comparisons. The maximum value of  $E_r$  at this range is  $5 \times 10^3$ . The maximum absolute value of  $B_\phi$  is  $3 \times 10^{-4}$ . In this case,  $F_m/e$  is  $\sim 8 \times 10^4$ . Since  $F_s/e$  is  $\sim 3.5 \times 10^5$ , it seems reasonable that the self-consistent effect on  $J_r$  due to  $E_r$  will be negligible, and the effect due to  $B_\phi$  will be small, particularly since at this range,  $|J_r| \gg |J_\theta|$  and nearly all the kinetic energy of the electron is in the radial direction.

The self-consistent theta currents for the two close-in ranges show three interesting features. First, while the non-self-consistent theta currents are always negative, the self-consistent theta currents are nearly always positive. Second, the self-consistent theta currents follow the prompt gamma pulse in a much more obvious fashion than the non-self-consistent theta currents. Third, after the prompt gamma pulse, the self-consistent theta currents dip and then exhibit a gentle bump, and finally change sign after 10 microseconds.

The self-consistent theta currents are nearly always positive because  $B_\phi$  nearly always predominates over  $E_\theta$  and the non-self-consistent  $J_r$  is nearly always greater than the non-self-consistent

$J_\theta$ . There is a very short span of time at very early times where  $E_\theta$  predominates. If values of  $E_\theta$  and  $F_m/e$  are compared at 3 shakes in the usual manner, the  $E_\theta$  dominance can be shown. In this tiny region of  $E_\theta$  dominance, the self-consistent theta currents are negative. This situation is shown in Figs. 5 and 14.

That the theta currents are almost entirely determined by  $B_\phi$  is further demonstrated by the jagged time behavior of  $E_\theta$  and consequent smearing of the prompt gamma pulse. In contrast, the theta currents are smooth and follow the gamma pulse quite well because close-in the shape of the gamma pulse is preserved in  $B_\phi$ .

Finally, the dip and gentle bump behavior is exhibited in  $B_\phi$  but, due to the obvious non-linear relationship of electron turning to the magnitude of  $B_\phi$ , the similarity of shape between the self-consistent  $J_\theta$  and  $B_\phi$  is not compelling, especially as the waveforms approach 10  $\mu$ sec where the non-self-consistent  $J_\theta$  becomes comparable to or greater than the non-self-consistent  $J_r$ . Beyond 10  $\mu$ sec  $J_\theta$  crosses over due to the fact that the non-self-consistent  $J_\theta$  becomes comparable to or greater than (at 500m) the non-self-consistent  $J_r$ . In this region the effect of  $B_\phi$  is to increase  $-J_r$ , as explained above, and so  $E_\theta$  dominates  $J_\theta$  behavior.  $E_\theta$  starts its dominance before 10  $\mu$ sec. The effect is to reverse  $J_\theta$ . At 12  $\mu$ sec and 500m (Fig. 9) and 22  $\mu$ sec and 1000m (Fig. 18)  $E_\theta$  crosses over and becomes positive. This causes the self-consistent  $J_\theta$  to hump over as it heads for another cross-over.

At 2000m, rough field comparison shows that  $E_\theta$  should dictate  $J_\theta$  behavior. First, a vestige of the gamma pulse is seen in  $J_\theta$ . The shape of the gamma pulse is preserved in  $E_\theta$  but not in  $B_\phi$ . Second,  $J_\theta$  is uniformly negative as is  $E_\theta$  past the start of the gamma pulse. Later in time  $B_\phi$  rises faster than  $E_\theta$  and at its peak there is a corresponding dip in  $J_\theta$  because, as shown earlier, a negative  $B_\phi$  acting on a negative  $J_r$  contributes to a positive  $J_\theta$ .

Now it remains to examine the effects of the self-consistent model on the fields and the conductivity.

SECTION IV  
THE EFFECT OF SELF-CONSISTENCY ON THE FIELDS

A few words should be said regarding the occasional raggedness of some of the fields. By examining range plots of  $E_\theta$ , it is clear that choosing the inner boundary condition  $E_\theta = 0$  is inappropriate. Originally this condition was chosen with the assumption that the inner boundary is a perfect conductor. This assumption is certainly inconsistent with the use of non-zero theta currents at the inner boundary. Range plots of  $E_\theta$  at early times show a drastic discontinuity between the inner boundary and the first point out in range. In fact,  $E_\theta$  is increasing in an exponential fashion toward the inner boundary rather than decreasing to zero. After a few time steps, this discontinuity develops into oscillations of  $E_\theta$  in range. In turn these oscillations affect  $J_\theta$  which feeds back into  $E_\theta$ . To minimize these oscillations, a range current smoother has been installed in SCX. This stopgap measure is helpful but not completely effective as can be seen in the time plots of near the prompt gamma pulse.

In addition, the calculation of the conductivity involves using a field dependent electron mobility which is clearly affected by the erratic behavior of  $E_\theta$ . The conductivity's slightly ragged behavior is fed back into  $E_r$  and into  $B_\phi$ . This problem should be cleared up, if not eliminated, by a more physically realistic choice of inner boundary condition for  $E_\theta$ , possibly something as simple-minded as:

$$E_\theta = -J_\theta/\sigma$$

The three equations of importance in SCX are, in retarded time, at  $\theta = 90^\circ$  (on the ground)

4

$$1) \quad \frac{1}{\mu r} \frac{\partial B_{\phi}}{\partial \theta} = J_r + \sigma E_r + \epsilon_0 \frac{\partial E_r}{\partial \tau}$$

$$2) \quad -\frac{1}{\mu r} \left[ \frac{\partial}{\partial r} (r B_{\phi}) - \frac{1}{c} \frac{\partial}{\partial \tau} (r B_{\phi}) \right] = J_{\theta} + \sigma E_{\theta} + \epsilon_0 \frac{\partial E_{\theta}}{\partial \tau}$$

$$3) \quad \frac{1}{r} \left[ \frac{\partial}{\partial r} (r E_{\theta}) - \frac{1}{c} \frac{\partial}{\partial \tau} (r E_{\theta}) - \frac{\partial}{\partial \theta} E_r \right] = -\frac{\partial B_{\phi}}{\partial \tau}$$

The usual arguments used to predict the time behavior of  $E_r$  from 1) are as follows. With the magnetic term negligible, at very early times  $J_r$ ,  $\sigma$  and  $E_r$  are very small and so  $\sigma E_r$  is negligible relative to  $J_r$ . Hence, the  $E_r$  behavior is predicted to be:  $E_r = -\frac{1}{\epsilon} \int J_r d\tau$ .

After a time,  $\sigma E_r$  becomes comparable to  $-J_r$ . Physically, this is described as occurring when the Compton current is cancelled by the conduction current. When this condition occurs  $\frac{\partial E_r}{\partial \tau}$  is negligible, assuming the effects of the airground asymmetry have not yet allowed  $B_{\phi}$  to diffuse into the region of interest. If  $J$  and  $\sigma$  rise initially as  $e^{\alpha t}$ ,  $E_r$  saturates, i.e.,  $\frac{\partial E_r}{\partial \tau}$  is small, for  $\sigma > \alpha \epsilon_0$ , where  $\epsilon_0$  is the free space permittivity. For an  $\alpha$  of  $2 \times 10^8$ , saturation occurs where  $\sigma > 1.77 \times 10^{-3}$  and the time of saturation can be determined by examining Figs. 6, 15 and 23. For 500 and 1000 meters, saturation occurs before the prompt gamma peak. At 2000 meters, saturation never occurs.

How accurately  $E_r$  follows  $-J_r/\sigma$  is estimated by a "relaxation time" which amounts to  $\epsilon_0/\sigma$ . If  $\sigma$  is large enough, the relaxation time is so short that  $E_r$  does in fact follow  $J_r/\sigma$ , most visibly at late times where  $J_r/\sigma$  changes. At far ranges or closer in at very late times,  $\sigma$  is so small that the relaxation time is too large to follow  $J_r/\sigma$ .



Furthermore, at the close-in ranges, 500 and 1000m, saturation occurs before the prompt gamma peak so that  $E_r$  also peaks, and at far ranges, 2000m, saturation occurs after the prompt gamma peak so that the peak is not preserved in  $E_r$  by following  $J_r/\sigma$ , but rather from  $E_r = \frac{-1}{\epsilon_0} \int J_r d\tau$ . For  $E_r$ , this results in a peak more broad and delayed in time from the prompt gamma peak. In certain time domains, some of these arguments are equally applicable to  $E_\theta$ .

At 500m and 1000m, saturation occurs before the prompt gamma peak. The plots of  $\sigma$  at these ranges show that the self-consistent model doesn't greatly change the conductivity. However,  $E_\theta$ , through the field-dependent electron mobility, introduces some small jaggedness into  $\sigma$ .

Since  $E_r = -J_r/\sigma$  until past neutron arrival where  $\sigma$  is greatly reduced, thus increasing the relaxation time, it is reasonable that the  $1/\sigma$  dependence of  $E_r$  greatly exaggerates the jaggedness in  $\sigma$ . Since  $J_r$  is reduced by self-consistency,  $E_r$  is reduced as well.

An interesting portion of the  $E_r$  curve is at and past neutron arrival. The  $\sigma$  curves show a sharp discontinuity in slope at neutron arrival and a subsequent characteristic hump.  $E_r$  exhibits this same slope discontinuity and an inverted hump out to about 30  $\mu$ sec.

Close in, before the prompt gamma peak,  $E_\theta$  is driven by the  $\frac{\partial}{\partial \tau}(rB_\phi)$  term. At 500m and 1000m, this can be readily seen. In both self-consistent and non-self-consistent plots of  $E_\theta$  there is a very smooth, sharp negative pulse which peaks at about 5 shakes. If this pulse were due to  $-J_\theta/\sigma$  the  $E_\theta$  pulse caused by a self-consistent  $J_\theta$  would be opposite in sign to the  $E_\theta$  pulse generated by a non-self-consistent  $J_\theta$ . Examination of the slope of the  $B_\phi$  curve shows that the  $E_\theta$  pulse is in fact driven by  $\frac{\partial}{\partial \tau}(rB_\phi)$ . Between 3 and 5 shakes,  $B_\phi$  rises rapidly and smoothly to a peak. Since  $B_\phi$  is negative, an increasing  $\frac{\partial}{\partial \tau}(rB_\phi)$  should give a negative  $E_\theta$  value. It is clear from the non-self-consistent plots of  $E_\theta$  that the pulse ends and a

sign change occurs at the point where  $B_\phi$  peaks and turns over. After  $B_\phi$  peaks, the slope of  $B_\phi$  doesn't do anything of great interest until neutron arrival. In the intervening interval,  $E_\theta$  is driven by  $-J_\theta/\sigma$  as can be accurately verified by comparing  $-J_\theta/\sigma$  with actual values of  $E_\theta$ .

An important difference shown in the overlay plots of  $E_\theta$  at 500m and 1000m is that, whereas  $E_\theta$  remains positive for a long time after the negative pulse for the non-self-consistent case,  $E_\theta$  remains negative for the self-consistent case. Here  $E_\theta$  is just following  $-J_\theta/\sigma$ .

At 2000m, an interesting feature is that while self-consistency reduces the magnitude of  $J_\theta$  due to  $B_\phi$ , the self-consistent  $E_\theta$  is actually larger than the non-self-consistent  $E_\theta$  at times greater than 10 shakes. Here  $E_\theta$  is not driven by  $J_\theta$ .

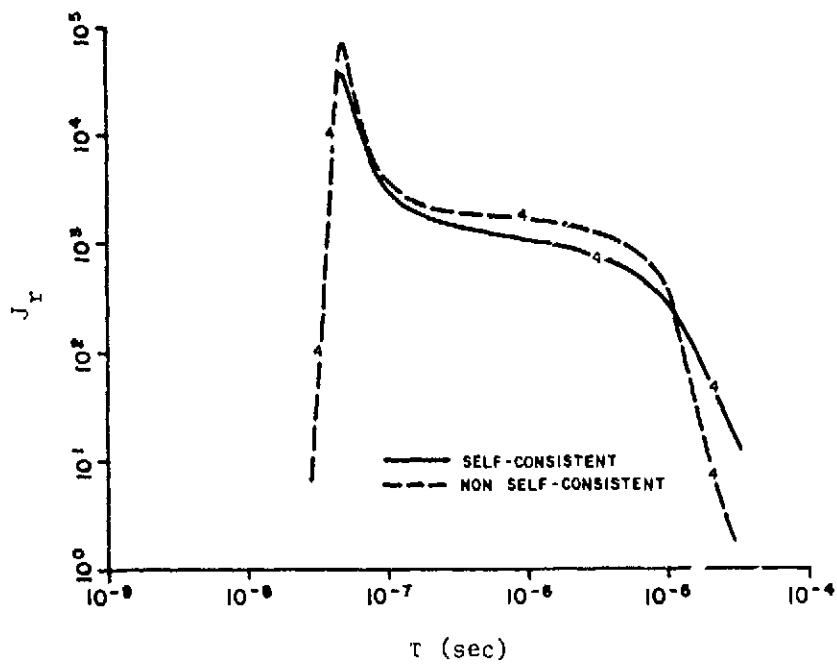


Fig. 3. Overlay of non-self-consistent and self-consistent radial currents at 500m, on the ground.

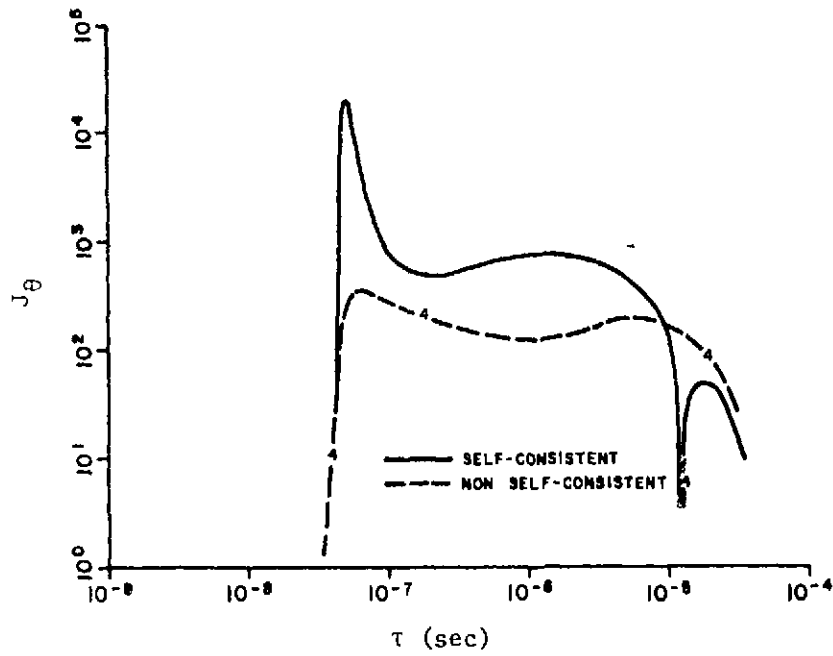


Fig. 4. Overlay, theta currents, 500m.

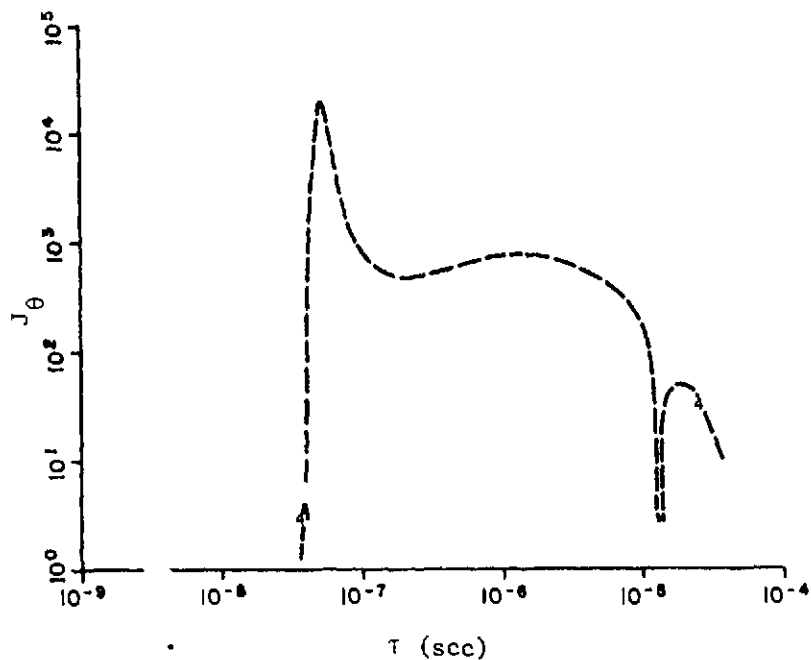


Fig. 5. Self-consistent theta current at 500m, on the ground.

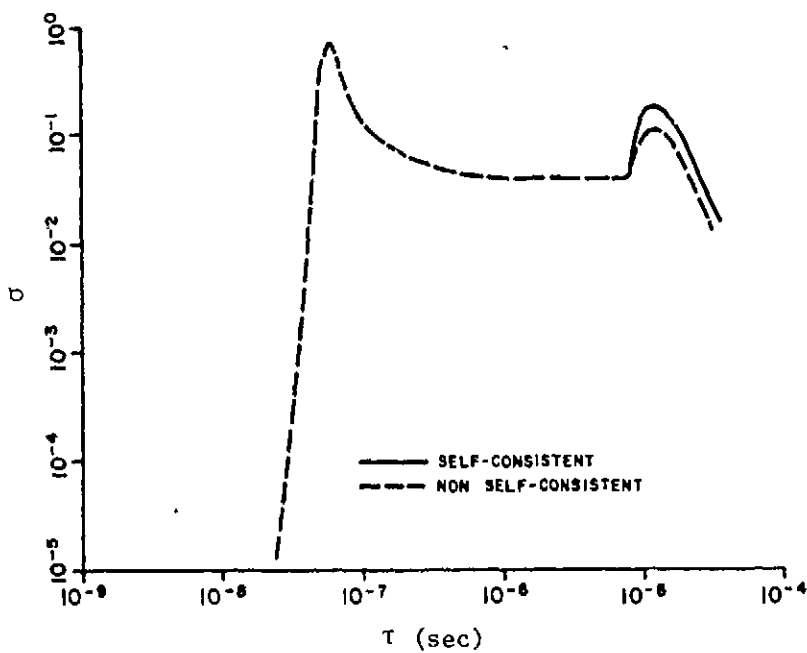


Fig. 6. Overlay, conductivities, 500m.

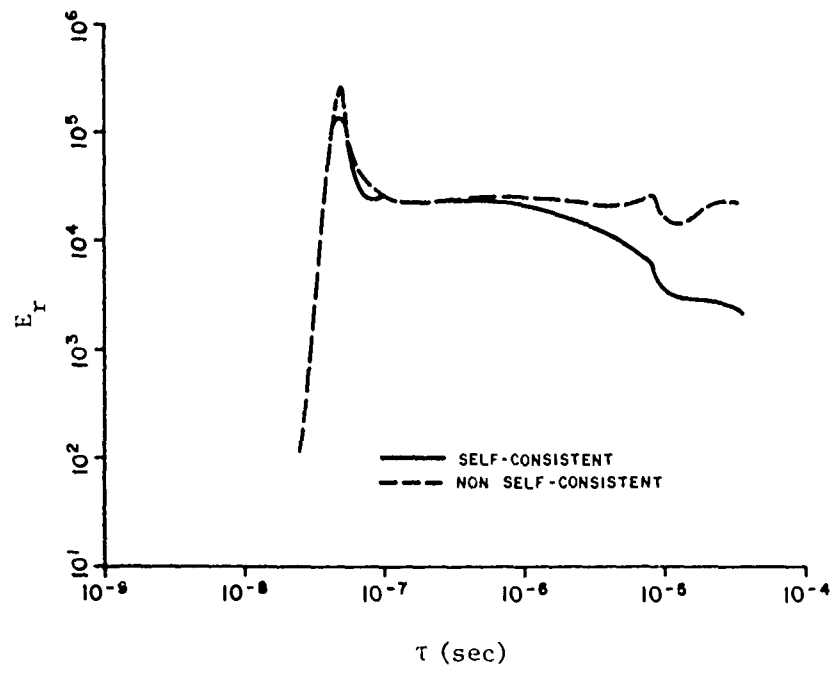


Fig. 7. Overlay, radial electric fields, 500m.

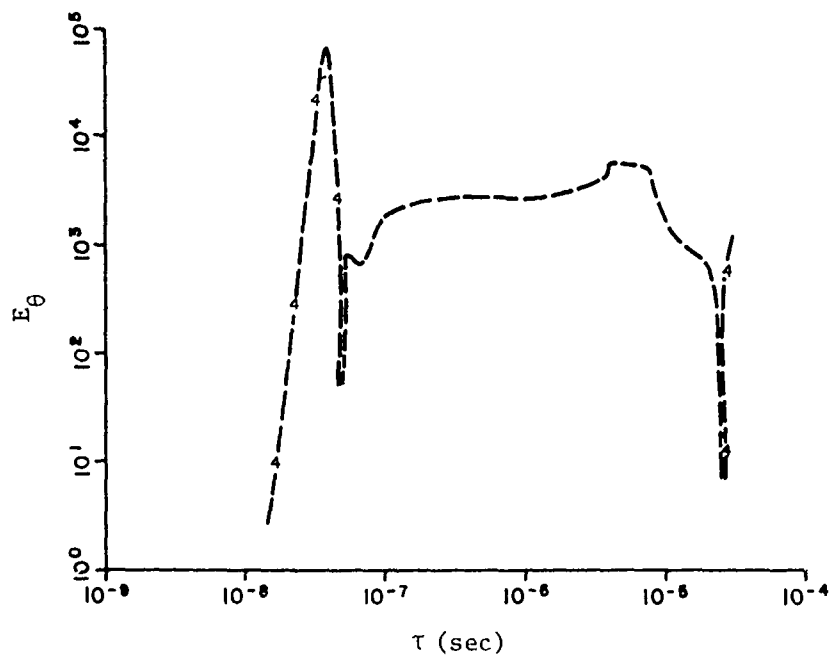


Fig. 8. Non-self-consistent theta electric field at 500m, on the ground.

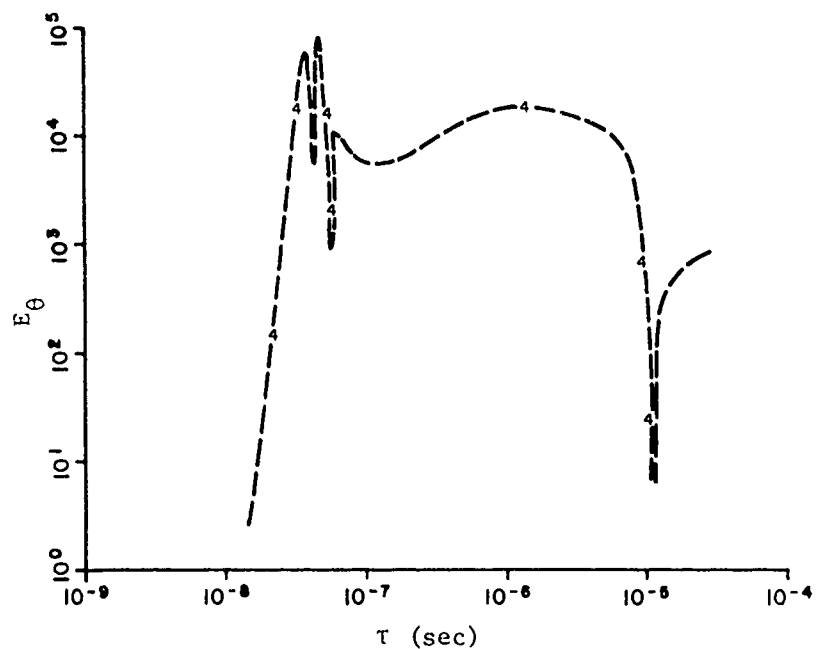


Fig. 9. Self-consistent theta electric field at 500m, on the ground.

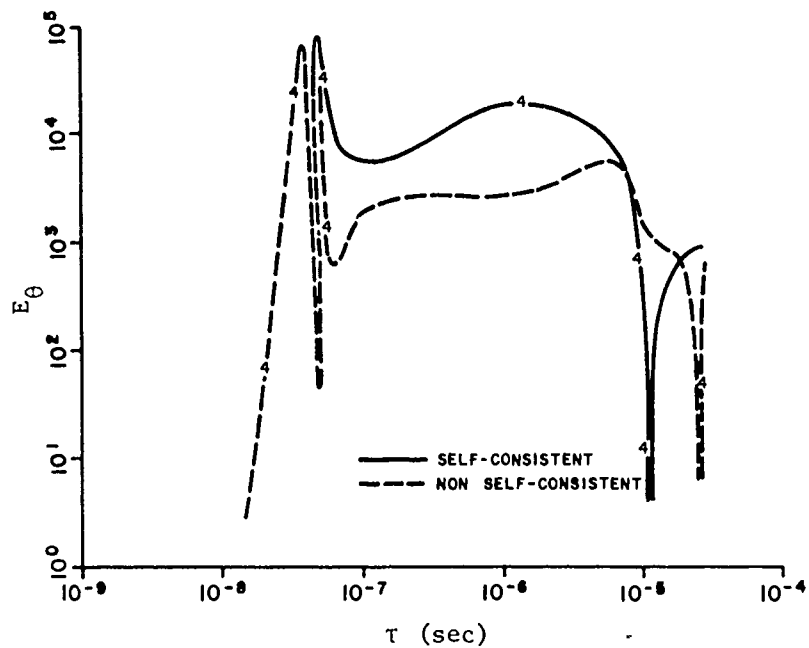


Fig. 10. Overlay, theta electric fields, 500m.

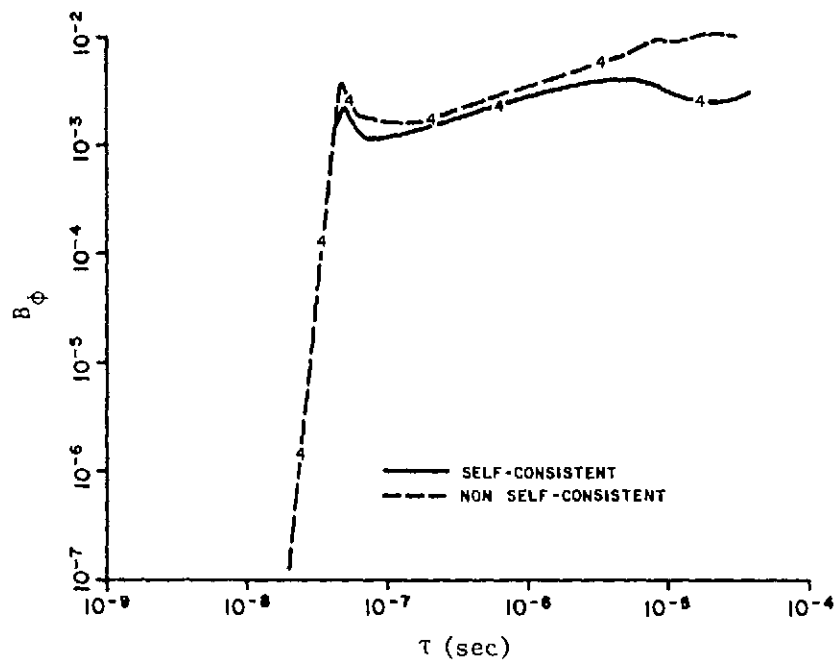


Fig. 11. Overlay, axial magnetic field, 500m.

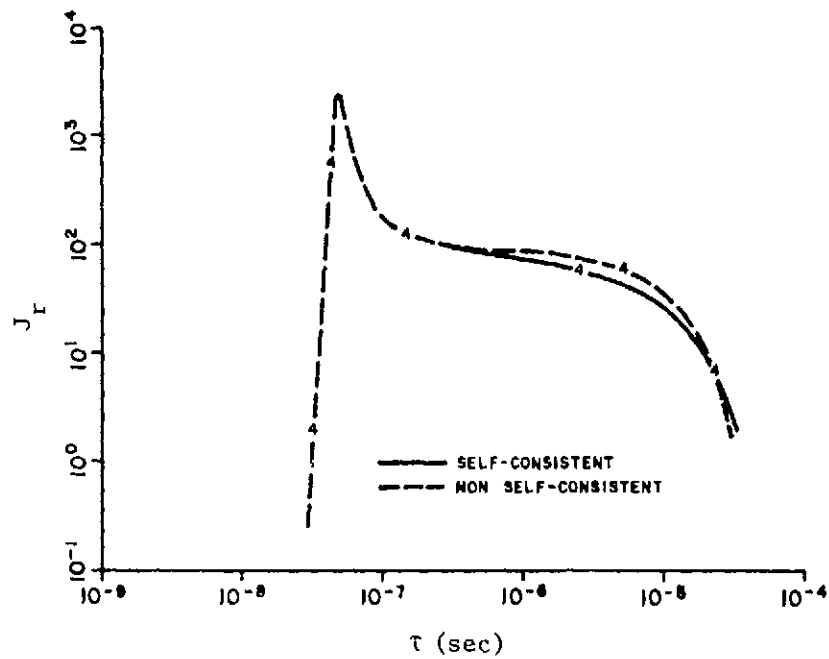


Fig. 12. Overlay, radial currents, 1000m.

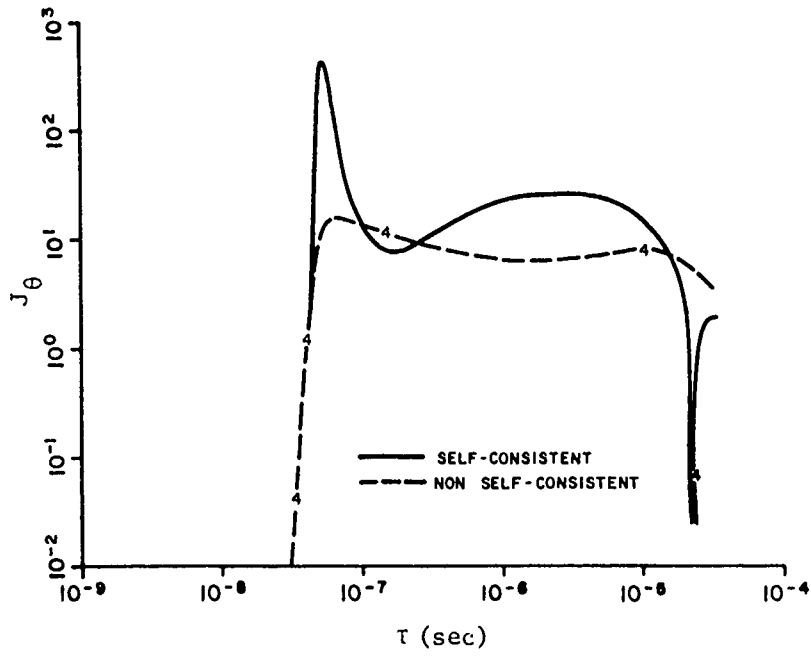


Fig. 13. Overlay, theta currents, 1000m.

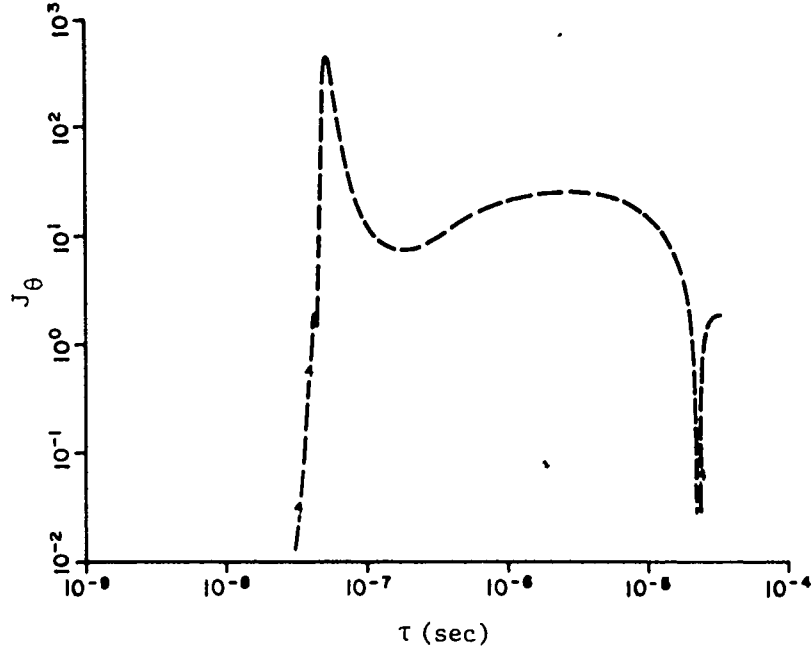


Fig. 14. Self-consistent theta current at 1000m, on the ground.



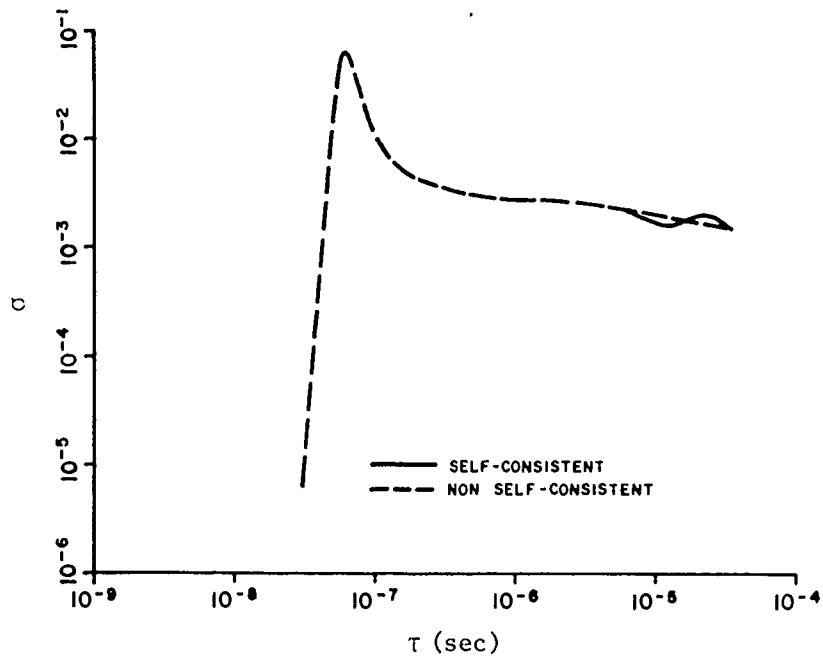


Fig. 15. Overlay, conductivities, 1000m.

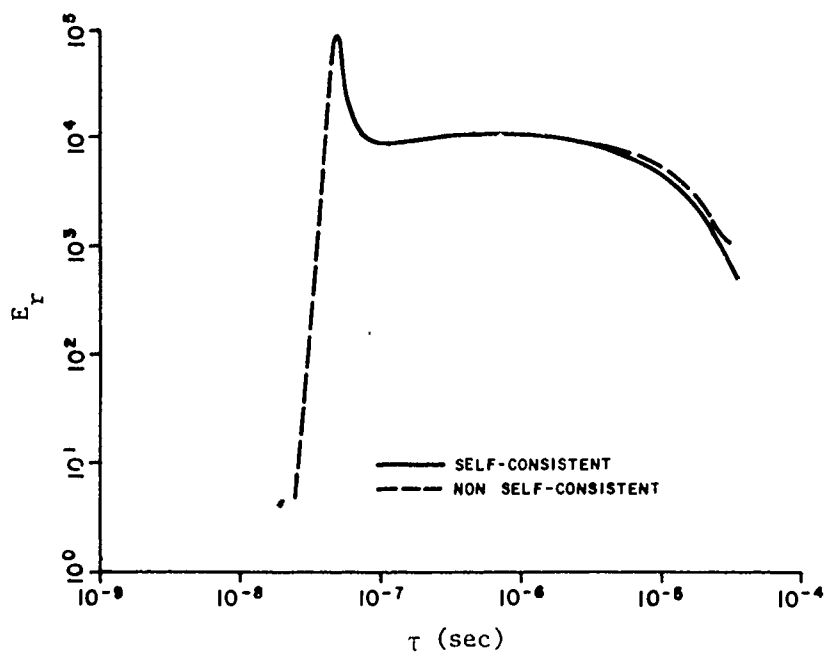


Fig. 16. Overlay, radial electric fields, 1000m.

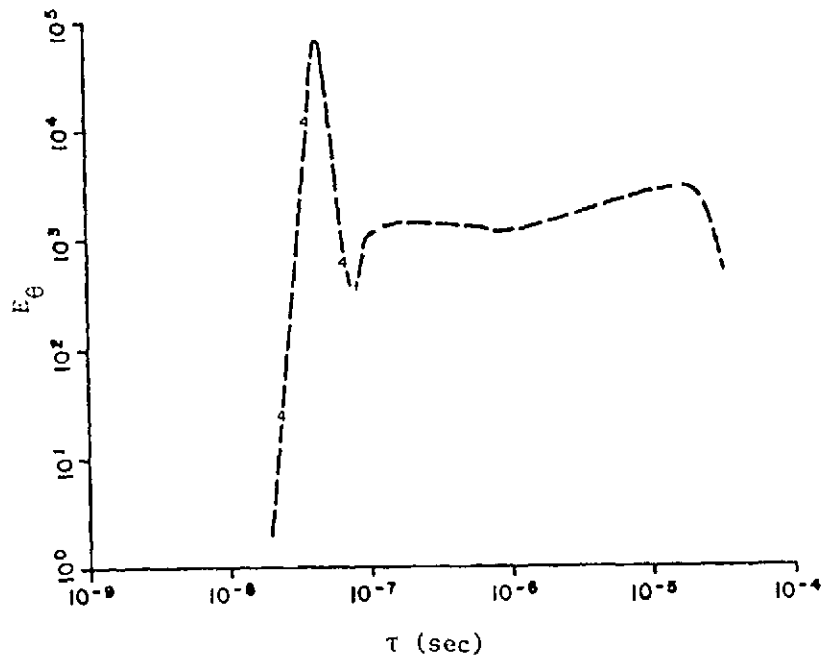


Fig. 17. Non-self-consistent theta electric field at 1000m, on the ground.

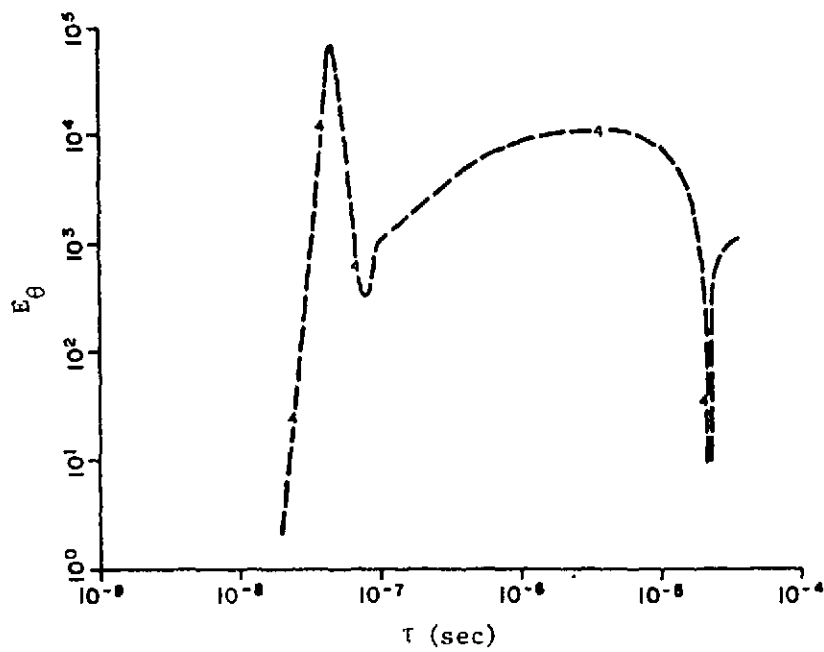


Fig. 18. Self-consistent theta electric field at 1000m, on the ground.

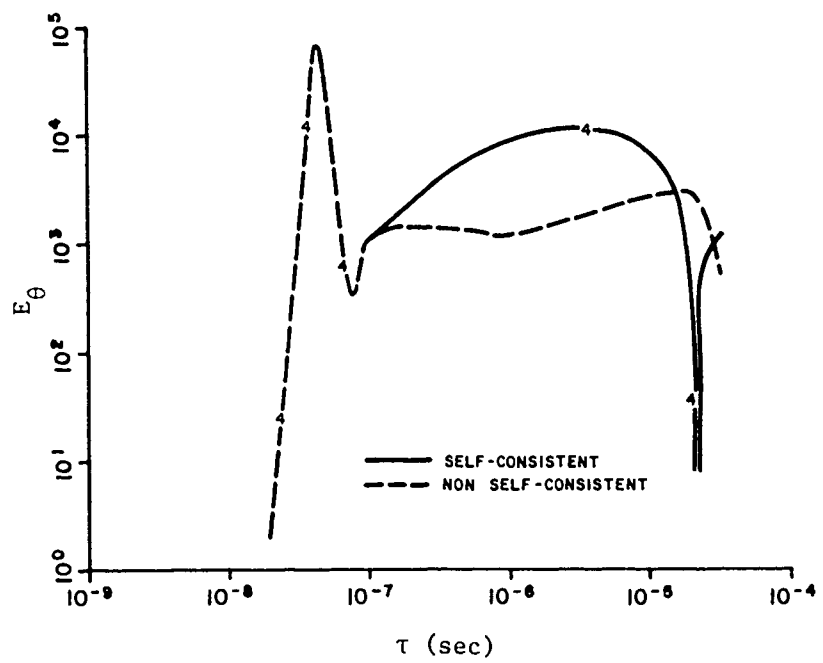


Fig. 19. Overlay, theta electric fields, 1000m.

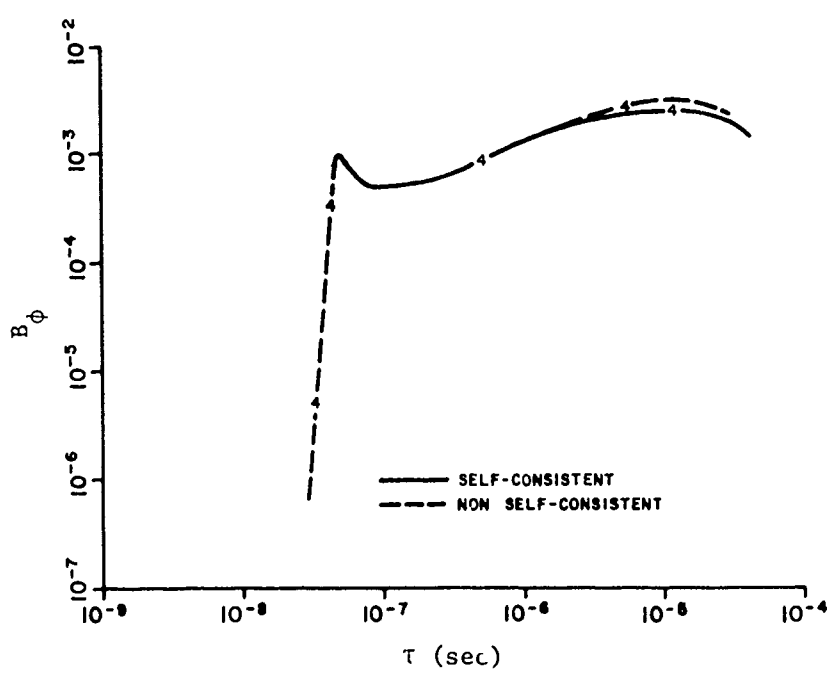


Fig. 20. Overlay, axial magnetic field, 1000m.

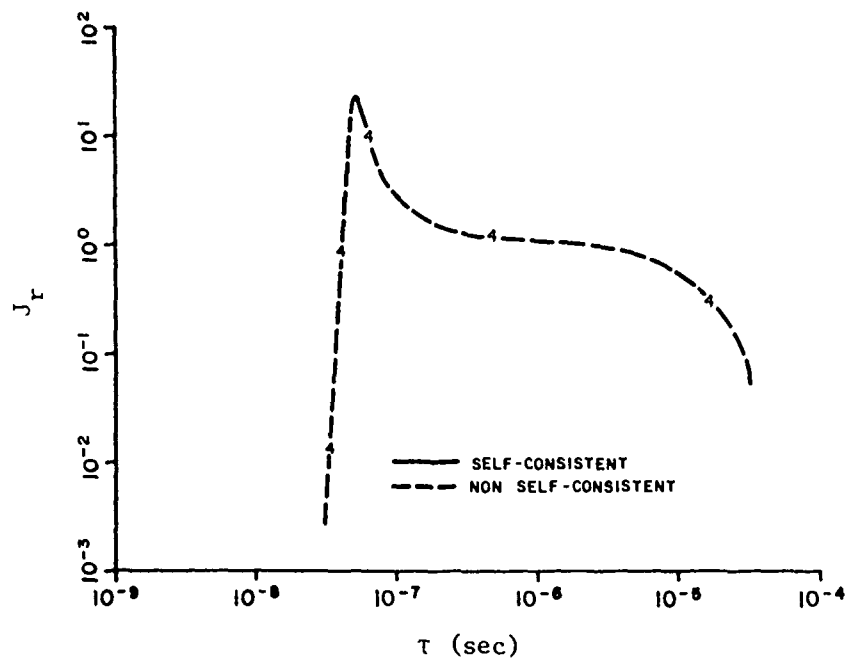


Fig. 21. Overlay, r dial currents, 2000m.

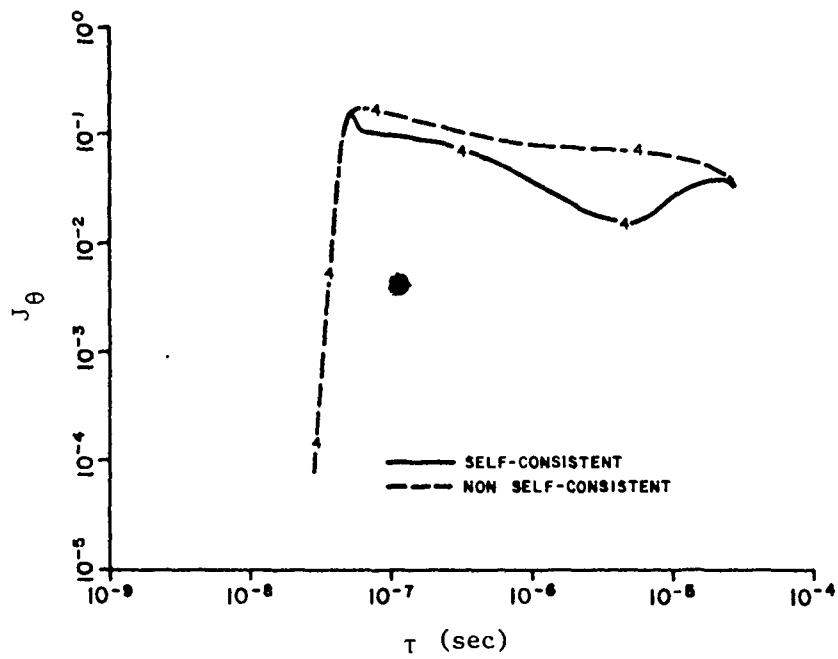


Fig. 22. Overlay, theta currents, 2000m.

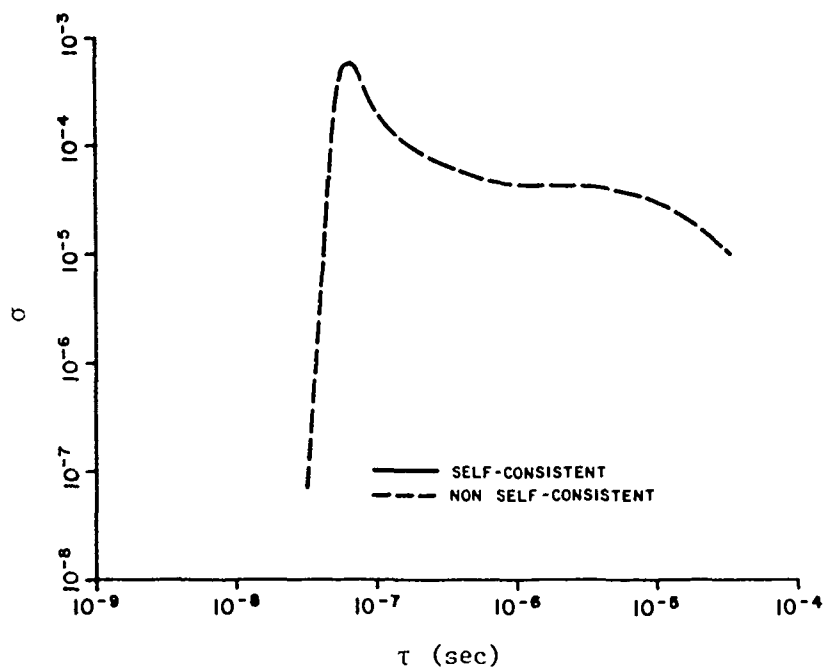


Fig. 23. Overlay, conductivity, 2000m.

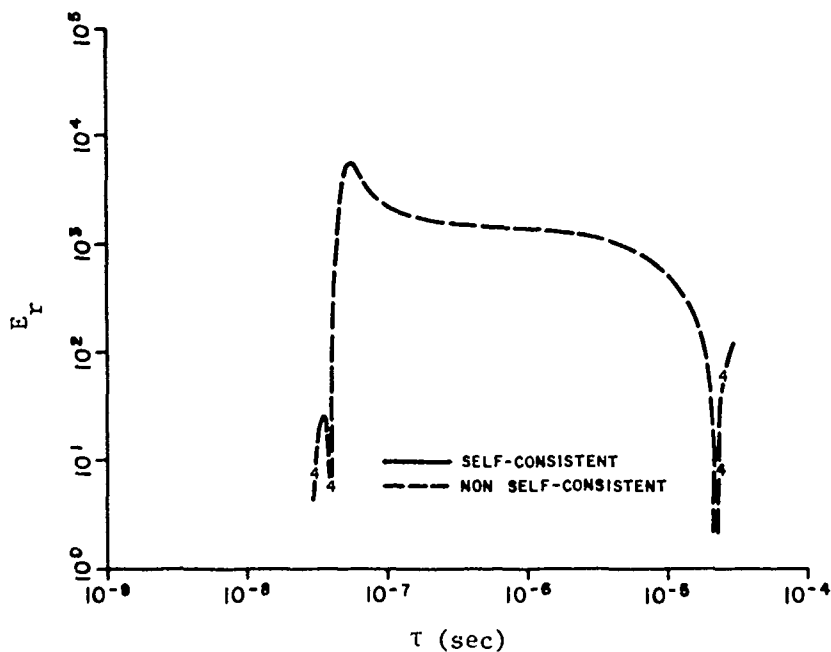


Fig. 24. Overlay, radial electric fields, 2000m.

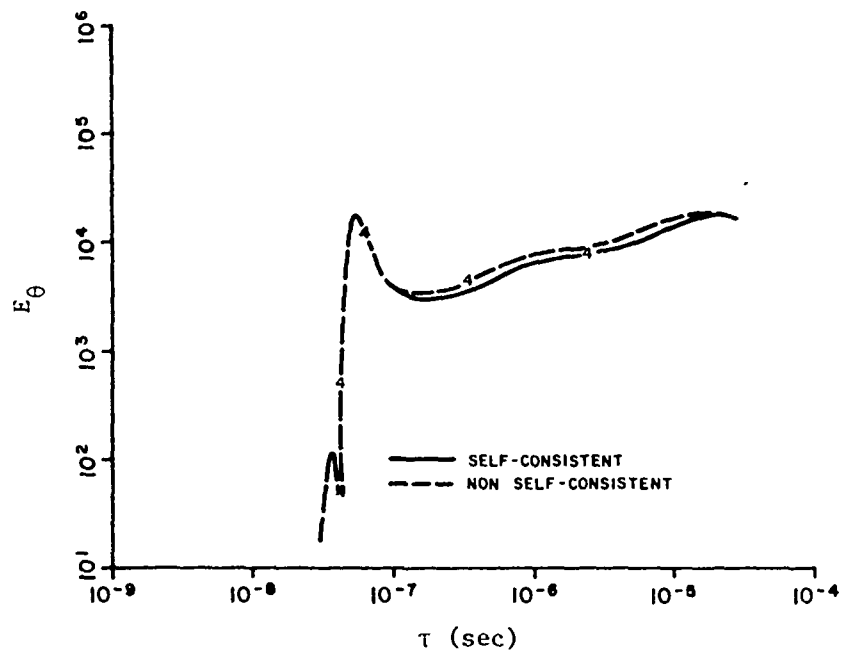


Fig. 25. Overlay, theta electric fields, 2000m.

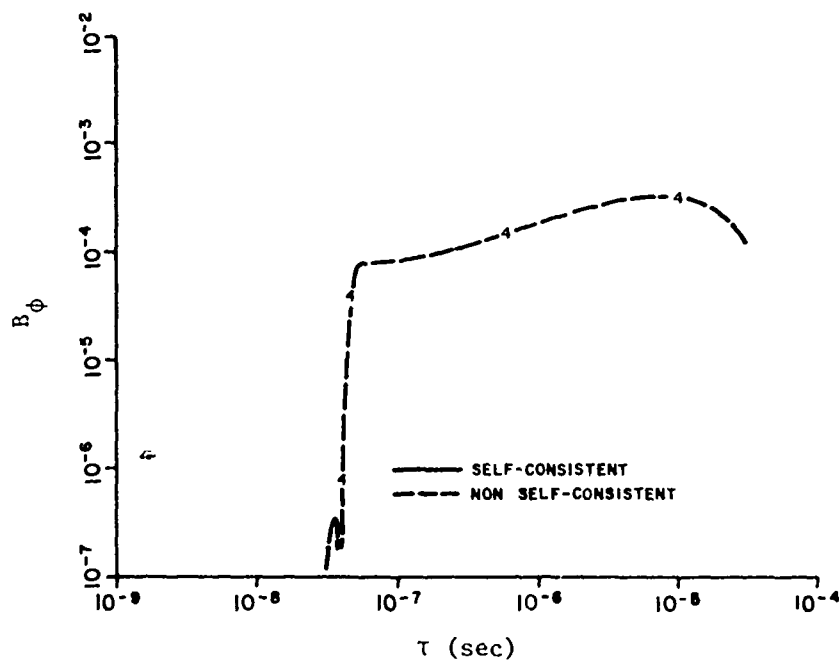


Fig. 26. Overlay, axial magnetic fields, 2000m.

## SECTION V

### RADIATION ENHANCED GROUND CONDUCTIVITY

In the past, SCX calculations have always assumed a uniform homogeneous ground with constant conductivity. However, in the real physical case, the deposition of radiation within the ground results in ionization which alters the conductivity from its ambient value. The time variation of the source and the nature of the deposition make the ground conductivity a function of both space and time. It is important to determine the effects of these possible variations on the EMP environments calculated with the SCX code.

To enhance calculational speed and efficiency, the coding in the SCX fields calculation has always implicitly assumed a constant ground conductivity. With the assumption of a variable conductivity, the differenced form of the radial equation in the ground becomes <sup>(3)</sup>

$$\begin{aligned} & \left( \frac{1}{c_g} + \sigma_{ij}^{hk} \mu_g \frac{\delta t}{2} \right) E_{\rho_{ij}}^{hk} - \left( \frac{Z(\rho, z)}{2} - \frac{\delta t}{2\delta z_j} \right) B_{\phi_{ij}}^k \\ & - \left( \frac{Z(\rho, z)}{2} + \frac{\delta t}{2\delta z_j} \right) B_{\phi_{ij-1}}^k = \left( \frac{1}{c_g} - \sigma_{ij}^{hk-1} \mu_g \frac{\delta t}{2} \right) E_{\rho_{ij}}^{hk-1} \\ & - \left( \frac{Z(\rho, z)}{2} + \frac{\delta t}{2\delta z_j} \right) B_{\phi_{ij}}^{k-1} - \left( \frac{Z(\rho, z)}{2} - \frac{\delta t}{2\delta z_j} \right) B_{\phi_{ij-1}}^{k-1} \end{aligned}$$

After the standard definition of constants, the following result is obtained

6

$$A1_j E_{\rho_{ij}}^{hk} - A21_j B_{\phi_{ij}}^k - A22_j B_{\phi_{ij-1}}^k = A3_j.$$

However, the following revised values of several constants must be used:

$$A1_j = \frac{1}{c_g} + \sigma_{ij}^{hk} \mu_g \frac{\delta t}{2}$$

$$A3_j = \left( \frac{1}{c_g} - \sigma_{ij}^{hk-1} \mu_g \frac{\delta t}{2} \right) E_{\rho_{ij}}^{hk-1}$$

$$-\left( \frac{Z(\rho, z)}{2} + \frac{\delta t}{2\delta z_j} \right) B_{\phi_{ij}}^{k-1} - \left( \frac{Z(\rho, z)}{2} - \frac{\delta t}{2\delta z_y} \right) B_{\phi_{ij-1}}^{k-1}$$

The other equation to be differenced which involves the conductivity is

$$R(\rho, z) \frac{\partial B_{\phi}}{\partial t} - \frac{1}{\rho} \frac{\partial}{\partial \rho} (\rho B_{\phi}) + \sigma \mu E_z \frac{1}{c_g} \frac{\partial E_z}{\partial \tau} = 0.$$

Assuming a variable conductivity, the following difference equation results



$$\begin{aligned}
& \left( R(\rho, z) - \frac{\rho_i}{\rho_i + \rho_{i-1}} \frac{\delta t}{\delta \rho} \right) B_{\phi_{ij}}^k + \left( \frac{1}{c_g} + \sigma_{ij}^k \mu_g \frac{\delta t}{2} \right) E_{z_{ij}}^k \\
& = \left( \frac{1}{c_g} - \sigma_{ij}^{k-1} \mu_g \frac{\delta t}{2} \right) E_{z_{ij}}^{k-1} + \left( R(\rho, z) - \frac{\rho_i}{\rho_i + \rho_{i+1}} \frac{\delta t}{\delta \rho} \right) B_{\phi_{ij}}^{k-1} \\
& \quad - \left( \frac{\rho_{i-1}}{\rho_i + \rho_{i-1}} \frac{\delta t}{\delta \rho} \right) B_{\phi_{i-1j}}^k + \left( \frac{\rho_{i+1}}{\rho_i + \rho_{i+1}} \frac{\delta t}{\delta \rho} \right) B_{\phi_{i+1j}}^k
\end{aligned}$$

Definition of constants results in

$$A4_j B_{\phi_{ij}}^k + A5_j E_{z_{ij}}^k = A6_j ,$$

However, the following constants require new definition

$$A5_j = \frac{1}{c_g} + \sigma_{ij}^k \mu_g \frac{\delta t}{2} \quad (\neq A1_j \text{ for this case})$$

$$\begin{aligned}
A6_j = & \left( \frac{1}{c_g} - \sigma_{ij}^{k-1} \mu_g \frac{\delta t}{2} \right) E_{z_{ij}}^{k-1} + \left( R(\rho, z) - \frac{\rho_i}{\rho_i + \rho_{i+1}} \frac{\delta t}{\delta \rho} \right) B_{\phi_{ij}}^{k-1} \\
& + \left( \frac{\rho_{i+1}}{\rho_i + \rho_{i+1}} \frac{\delta t}{\delta \rho} \right) B_{\phi_{i+1j}}^{k-1} - \left( \frac{\rho_{i-1}}{\rho_i + \rho_{i-1}} \frac{\delta t}{\delta \rho} \right) B_{\phi_{i-1j}}^k .
\end{aligned}$$

When these changes are included in the field calculation subroutine of SCX, the effect of radiation enhanced ground conductivity may be examined.

Numerous models have been proposed to approximate the behavior of the ground conductivity with dose. To estimate the nature of the effect in SCX, it is convenient to use a simple model suggested by Graham and used by Jones<sup>(3)</sup>. In this approximation

$$\sigma_g(Q, z) = \sigma_g(\text{constant}) + \frac{1 \times 10^{-14}}{8.081 \times 10^{10}} \frac{34}{10^6} Q e^{20z}$$

where

$Q$  is the ionization rate at the ground

$$8.081 \times 10^{10} \frac{\text{mev}}{\text{m}^3} = 1 \text{ rad air}$$

$z$  is the depth in meters (a negative number), and

$\sigma_g(\text{constant})$  is the normal ground conductivity.

For a source on the ground, as is the case in SCX, the deposition beneath the surface is rather small for ranges greater than a few hundred meters. A typical value for the ground conductivity in SCX calculations is 0.01 mhos/meter. Figure 1 shows the radiation enhanced conductivity as a function of time 5 cm below the surface at a range of 250 meters in a typical SCX run. It can be seen that the values change by at most about 50% near the peak. Near the prompt peak, values of the transverse electric field on the

ground decrease by up to 30% for an observer at 250 meters. By 500 meters, the decrease is more like 5%. For the farther observers, the time histories compare within a line width. Thus, except for very close in observers there is little or no effect of enhanced conductivity on SCX results. This was the expected result for a ground burst due to the very small deposition in the ground. For a near surface case where the deposition can be orders of magnitude greater for down range observers, significant results would be expected.

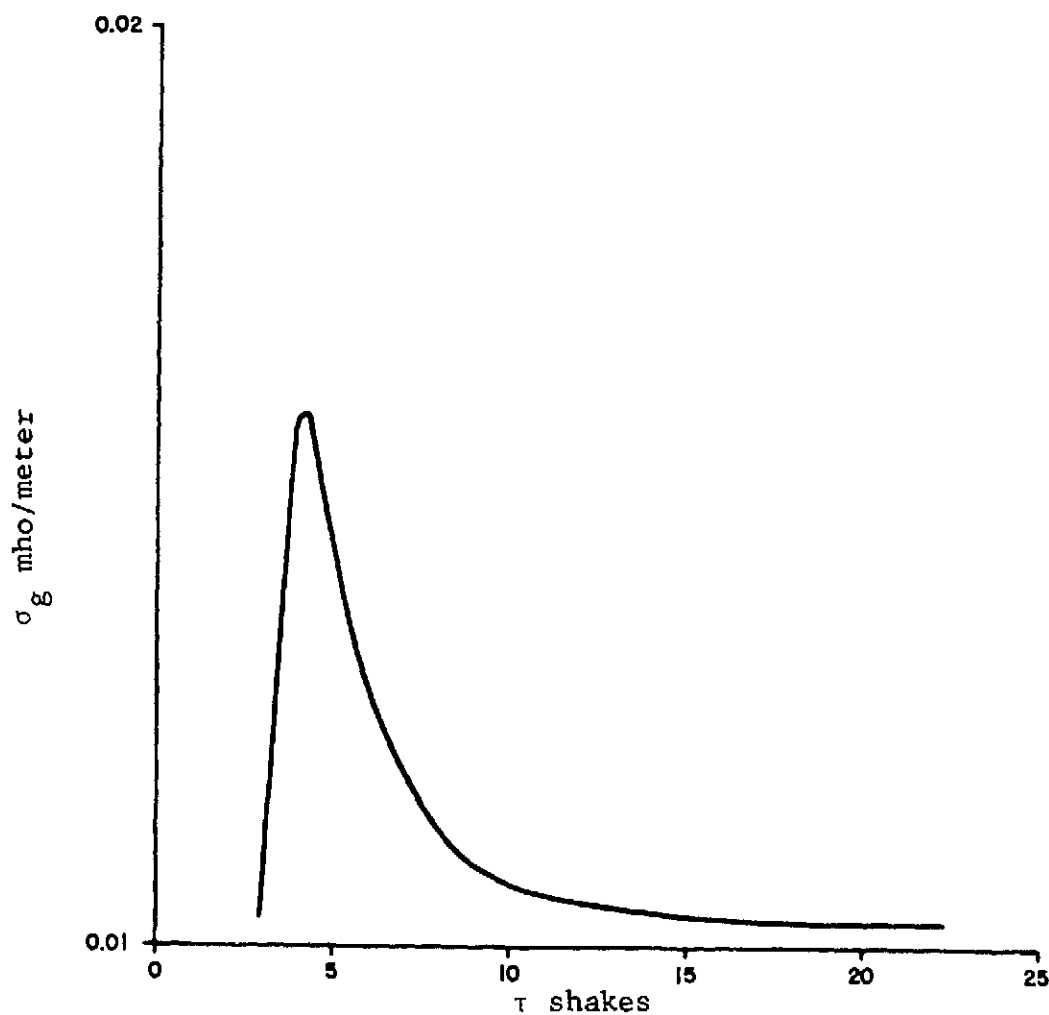


Figure 27. Radiation Enhanced Ground Conductivity vs. Time for Range of 250m and Depth of .05m.

## REFERENCES

1. Dalich, S. J., "SCX: A Two-Dimensional Ground Burst EMP Code," SAI-73-501-AQ, June 1973.
2. Longley, H. J., "Compton Current in Presence of Fields for LEMP 1," EMP Theoretical Note 77, Vol. 2-4.
3. Jones, C. W., "EMP Comparisons of Photon Transport in the Vicinity of a Material Interface with Photon Transport in a Homogeneous Atmosphere," DC-TN-2153-2, 1972.

## DISTRIBUTION LIST

### DEPARTMENT OF DEFENSE

Director  
Armed Forces Radiobiology Research Institute  
Defense Nuclear Agency  
ATTN: Technical Library  
ATTN: Robert E. Carter

Assistant to the Secretary of Defense  
Atomic Energy  
ATTN: Document Control

Director  
Defense Advanced Research Project Agency  
ATTN: Technical Library  
ATTN: AD/E&PS, George H. Halmeier  
ATTN: NMR

Director  
Defense Civil Preparedness Agency  
ATTN: TS AED  
ATTN: RE EO  
ATTN: Technical Library

Defense Communication Engineer Center  
ATTN: Code R-720, C. Stansberry  
ATTN: Code R-410, James W. McLean  
ATTN: Code R-400  
ATTN: Code R-124C, Technical Library

Director  
Defense Communications Agency  
ATTN: Code 950  
ATTN: Technical Library  
ATTN: Code 430  
ATTN: Code 930, Franklin D. Moore  
ATTN: Code 930, Monte I. Burgett, Jr.

Defense Documentation Center  
12 cy ATTN: TC

Commander  
Defense Electronic Supply Center  
ATTN: ECS  
ATTN: EQ  
ATTN: Technical Library

Director  
Defense Intelligence Agency  
ATTN: DI-7D, Edward O'Farrell  
ATTN: DI-7D  
ATTN: DI-3  
ATTN: Technical Library

Director  
Defense Nuclear Agency  
ATTN: STSI, Archives  
ATTN: RAAE  
ATTN: DDSI  
ATTN: RATN  
ATTN: RAEV  
ATTN: STVL  
ATTN: PPSR  
2 cy ATTN: SPSS  
2 cy ATTN: STAP  
5 cy ATTN: SPAS, D. Kohler  
2 cy ATTN: STTL, Technical Library

### DEPARTMENT OF DEFENSE (Continued)

Headquarters  
European Command  
ATTN: Technical Library

Commander  
Field Command  
Defense Nuclear Agency  
ATTN: FCPR

Director  
Interservice Nuclear Weapons School  
ATTN: Document Control  
ATTN: Technical Library

Director  
Joint Strategic Target Planning Staff, JCS  
ATTN: JSAS  
ATTN: JLTW-2  
ATTN: STINFO Library

Chief  
Livermore Division, Field Command, DNA  
ATTN: Document Control for L-395  
ATTN: FCPRL

National Communications System  
ATTN: NCS-TS, Charles D. Bodson

DDR&E  
ATTN: Asst. Dir., Strat. Wpns.

Director  
National Security Agency  
ATTN: Technical Library  
ATTN: TDL  
ATTN: Orland O. Van Gunten, R-425

OJCS/J-6  
ATTN: J-6, ESD-2

Director  
Telecommunications & Command & Control System  
ATTN: AD/ODTACCS  
ATTN: Dep. Asst., Sec. Sys.

Commander-in-Chief  
U.S. European Command, JCS  
ATTN: Technical Library

Weapons Systems Evaluation Group  
ATTN: Document Control

### DEPARTMENT OF THE ARMY

Asst. Chief of Staff for Intelligence  
ATTN: DAMA-TAS, Jack T. Blackwell

Commander  
Ballistic Defense System Command  
ATTN: Technical Library  
ATTN: BDMSC-TEN, Noah J. Hurst

Director  
Ballistic Missile Defense Advanced Technical Center  
ATTN: Technical Library

DEPARTMENT OF THE ARMY (Continued)

Chief of Research, Development & Acquisition  
Department of the Army  
ATTN: DAMA-CSM-N, LTC L. V. DeBoeser, Jr.

Commander  
Harry Diamond Laboratories  
ATTN: AMXDO-TI, Technical Library  
ATTN: AMXDO-EM, Ron Bostak  
ATTN: AMXDO-EM, John Bombardt  
ATTN: AMXDO-RB, Joseph R. Miletta  
ATTN: AMXDO-TR, Edward E. Conrad  
ATTN: AMXDO-EM, William T. Wyatt, Jr.  
ATTN: AMXDO-NP, Francis N. Wimenitz  
ATTN: AMXDO-RBI, John A. Rosado  
ATTN: AMXDO-RB, Robert E. McCoskey  
ATTN: AMXDO-RCC, John E. Thompkins

Commander  
Picatinny Arsenal  
ATTN: SMUPA-ND-W  
ATTN: SARPA-ND-C-E, Amina Nordio  
ATTN: SMUPA-TN, Barton V. Franks  
ATTN: Paul Harris  
ATTN: Technical Library  
ATTN: SMUPA-ND-D-C-2  
ATTN: SARPA-TS-I-E, Abraham Grinoch

Commander  
Redstone Scientific Information Center  
4 cy ATTN: AMSMI-RBD, Clara T. Rogers

Commander  
U. S. Army Armor Center  
ATTN: ATSAR-CD-MS  
ATTN: Technical Library

Director  
U. S. Army Ballistic Research Laboratories  
ATTN: AMXBR-AM, W. R. VanAntwerp  
ATTN: AMXBR-VL, John W. Kinch  
ATTN: AMXRD-BVL, David L. Rigotti  
ATTN: AMXBR-X, Julius J. Meszaros  
ATTN: Technical Library, Edward Baicy

U. S. Army Communications Command  
C-E Services Division  
ATTN: CEEO-7, Wesley T. Heath, Jr.

Commander  
U. S. Army Communications Command  
ATTN: Technical Library

Commander  
U. S. Army Communications Command  
ATTN: ACCM-TD-A, Library

Chief  
U. S. Army Communications System Agency  
ATTN: SCCM-AD-SV, Library

Commander  
U. S. Army Computer Systems Command  
ATTN: Technical Library

Commander Officer  
U. S. Army Electronics Command  
ATTN: Technical Library

DEPARTMENT OF THE ARMY (Continued)

Commander  
U. S. Army Electronics Command  
ATTN: AMSEL-NI-D  
ATTN: AMSEL-CE, T. Preiffer  
ATTN: AMSEL-CT-HDK, Abraham E. Cohen  
ATTN: AMSEL-GG-TD, W. R. Werk  
ATTN: AMSEL-WL-D  
ATTN: AMSEL-TL-MD, Gerhart K. Gaule  
ATTN: AMSEL-TL-ME, M. W. Pomerantz  
ATTN: AMSEL-TL-IR, Robert A. Freiberg  
ATTN: AMSEL-PL-ENV, Hans A. Bomke

Commander  
U. S. Army Electronics Proving Ground  
ATTN: STEEP-MT-M, Gerald W. Durbin

Division Engineer  
U. S. Army Engr. Dist. Missouri River  
ATTN: MRDED-MC, Floyd L. Hazlett

Commander-in-Chief  
U. S. Army Europe & Seventh Army  
ATTN: Technical Library

Commandant  
U. S. Army Field Artillery School  
ATTN: ATSFAC-CTD-MI, Harley Moberg  
ATTN: Technical Library

Commander  
U. S. Army Mat. & Mechanics Research Center  
ATTN: AMXMR-III, John F. Dignam  
ATTN: Technical Library

Director  
U. S. Army Material Sys. Analysis Agency  
ATTN: AMXSY-CC, Donald R. Barthel  
ATTN: Technical Library

Commander  
U. S. Army Materiel Command  
ATTN: AMCRD-WN-RE, John F. Corrigan  
ATTN: Technical Library

Commander  
U. S. Army Missile Command  
ATTN: AMSMI-RGD, Vic Ruwe  
ATTN: AMCPM-LCEX, Howard H. Henriksen  
ATTN: AMCPM-PE-EG, William B. Johnson  
ATTN: AMSMI-RGP, Hugh Green  
ATTN: AMCPM-PE-EA, Wallace O. Wagner  
ATTN: Technical Library

Commander  
U. S. Army Mobility Equip. R&D Center  
ATTN: STSFB-MW, John W. Bond, Jr.  
ATTN: Technical Library

Commander  
U. S. Army Nuclear Agency  
ATTN: ATCN-W, LTC Leonard A. Sluga  
ATTN: Technical Library

Commander  
U. S. Army Security Agency  
ATTN: IARD-T, Robert H. Burkhardt  
ATTN: Technical Library

DEPARTMENT OF THE ARMY (Continued)

Commandant  
U.S. Army Southeastern Signal School  
ATTN: Technical Library  
ATTN: ATSO-CTD-CS, CPT G. M. Alexander

Project Manager  
U.S. Army Tactical Data Systems, AMC  
ATTN: Technical Library

Commander  
U.S. Army Tank Automotive Command  
ATTN: Technical Library  
ATTN: AMCPM-GCM-SW, Lyle A. Wolcott

Commander  
U.S. Army Test & Evaluation Command  
ATTN: AMSTE-NB, Russell R. Galasso  
ATTN: AMSTE-EL, Richard I. Kolchin  
ATTN: Technical Library

Commander  
U.S. Army Training & Doctrine Command  
ATTN: Technical Library  
ATTN: ATORI-OP-SD

Commander  
White Sands Missile Range  
ATTN: STEWS-TE-NT, Marvin P. Squires  
ATTN: Technical Library

DEPARTMENT OF THE NAVY

Chief of Naval Operations  
Navy Department  
ATTN: Code 604C3, Robert Piacesi

Chief of Naval Research  
Navy Department  
ATTN: Code 464, Thomas P. Quinn  
ATTN: Code 127  
ATTN: Technical Library

Officer-in-Charge  
Civil Engineering Laboratory  
ATTN: Technical Library  
ATTN: Code L-31

Commander  
Naval Air Systems Command  
Headquarters  
ATTN: Technical Library  
ATTN: AIR-350F, LCDR Hugo Hart

Commanding Officer  
Naval Ammunition Depot  
ATTN: Technical Library  
ATTN: Code 7024, James Ramsey

Commander  
Naval Electronic Systems Command  
Naval Electronic Systems Command Headquarters  
ATTN: PME 117-T  
ATTN: PME 117-215A, Gunter Brunhart  
ATTN: PME 117-21  
ATTN: Technical Library

DEPARTMENT OF THE NAVY (Continued)

Commander  
Naval Electronics Laboratory Center  
ATTN: Code 2200, Verne E. Hildebrand  
ATTN: Code 3100, E. E. McCown  
ATTN: Code 2100, S. W. Lichtman  
ATTN: Technical Library

Commanding Officer  
Naval Intelligence Support Center  
ATTN: NISC-45  
ATTN: Technical Library

Superintendent  
Naval Postgraduate School  
ATTN: Code 2124, Technical Reports Librarian

Director  
Naval Research Laboratory  
ATTN: Code 2627, Doris R. Folen  
ATTN: Code 2027, Technical Library  
ATTN: Code 4004, Emanuel L. Brancato  
ATTN: Code 6631, James C. Ritter  
ATTN: Code 7706, Jay P. Boris  
ATTN: Code 7701, Jack D. Brown  
ATTN: Code 7770, Leslie S. Levine  
ATTN: Code 461, R. Gracen Joiner

Commander  
Naval Sea Systems Command  
Navy Department  
ATTN: SEA-9931, Riley B. Lane

Commander  
Naval Ship Engineering Center  
ATTN: Technical Library  
ATTN: Code 6174D2, Edward F. Duffy

Commander  
Naval Surface Weapons Center  
ATTN: Code 1224, Navy Nuc. Prgms. Off.  
ATTN: Code 431, John H. Malloy  
ATTN: Code WR-43  
ATTN: Code 431, Edwin R. Rathburn  
6 cy ATTN: Code 730, Technical Library

Commander  
Naval Surface Weapons Center  
ATTN: Technical Library

Commander  
Naval Telecommunications Command  
ATTN: Technical Library

Commander  
Naval Weapons Center  
ATTN: Code 533, Technical Library

Commanding Officer  
Naval Weapons Evaluation Facility  
ATTN: Lawrence R. Oliver  
ATTN: Code ATG, Mr. Stanley  
ATTN: ADS

DEPARTMENT OF THE NAVY (Continued)

Commanding Officer  
Navy Astronautics Group  
ATTN: Technical Library

Commanding Officer  
Nuclear Weapons Training Center, Pacific  
ATTN: Code 50

Director  
Strategic Systems Project Office  
Navy Department  
ATTN: NSP-43, Technical Library  
ATTN: NSP-2431, Gerald W. Hoskins  
ATTN: NSP-230, David Gold  
ATTN: SP-2701, John W. Pitsenberger

Commander  
U.S. Naval Coastal Systems Laboratory  
ATTN: Technical Library

Commander-in-Chief  
U.S. Pacific Fleet  
ATTN: Document Control

DEPARTMENT OF THE AIR FORCE

Commander  
ADC/DE  
ATTN: DEEDS, Joseph C. Brannan  
ATTN: DDEEN

Commander  
ADC/XZ  
ATTN: XPQDQ, Maj G. Kuch  
ATTN: XPDQ

Commander  
Aeronautical Systems Division, AFSC  
ATTN: Technical Library

AF Armament Laboratory, AFSC  
ATTN: DLOSL, Library

AF Cambridge Research Laboratories, AFSC  
ATTN: J. Emery Cormier

AF Weapons Laboratory, AFSC  
ATTN: ELP, William Page  
ATTN: ELP, Carl E. Baum  
ATTN: HO, Dr. Minge  
ATTN: DYV, Maj Mitchell  
ATTN: DYV, Capt Scammon  
ATTN: DYV, Lt Mac Farlane  
ATTN: DYX, Donald C. Wunsch  
ATTN: EL, John Darrah  
ATTN: ELA, J. P. Castillo  
ATTN: SAT  
ATTN: SAB  
ATTN: EL  
ATTN: EL, Library  
ATTN: DY  
ATTN: DYV, Maj Stuber  
ATTN: DYV, Dr. Place  
ATTN: DYV, Mr. Bick  
2 cy ATTN: SUL

AFISC  
ATTN: PQAL

DEPARTMENT OF THE AIR FORCE (Continued)

AFTAC  
ATTN: Technical Library  
ATTN: TAP

Air Force Avionics Laboratory, AFSC  
ATTN: Technical Library

AUL  
ATTN: LDE

AFML  
ATTN: Technical Library

Dir. Nuc. Safety  
ATTN: SN

Headquarters  
Air Force Systems Command  
ATTN: Technical Library

Commander  
Air University  
ATTN: AUL/LSE-70-250

Headquarters  
Electronic Systems Division, AFSC  
ATTN: Technical Library  
ATTN: YWEI  
ATTN: XRT, Lt Col John M. Jasinski  
ATTN: YSEV, Lt Col David C. Sparks

Commander  
Foreign Technology Technology Division, AFSC  
ATTN: TD-BTA, Library  
ATTN: ETET, Capt Richard C. Husemann

HQUSAF/RD  
ATTN: RDQPX

Commander  
Ogden Air Logistics Center  
ATTN: MMEWM, Robert Joffs  
ATTN: Technical Library

Commander  
Rome Air Development Center, AFSC  
ATTN: EMTLD, Document Library

Commander  
Sacramento Air Logistics Center  
ATTN: Technical Library

SAMSO/MN  
ATTN: MNNH, Capt Michael V. Bell  
ATTN: MNNH, Capt B. Stewart  
ATTN: MNNR

SAMSO/RS  
ATTN: RSSE  
ATTN: Technical Library

SAMSO/SK  
ATTN: SKF, Peter H. Stadler

SAMSO/YD  
ATTN: YDD, Maj Marion F. Schneider

USAF  
SCLO  
ATTN: Maj J. H. Pierson, Chief, LO



DEPARTMENT OF THE AIR FORCE (Continued)

Commander in Chief  
Strategic Air Command  
ATTN: DEF, Frank N. Bousha  
ATTN: NRI-STINFO Library  
ATTN: XPFS, Maj Brian G. Stephan

544th IES  
ATTN: RDPO, Lt Alan B. Merrill

ENERGY RESEARCH & DEVELOPMENT ADMINISTRATION

Division of Military Application  
U.S. Energy Research & Development Administration  
ATTN: Document Control for Class. Tech. Lib.

EG&G, Inc.  
Los Alamos Division  
ATTN: L. Deteh  
ATTN: Technical Library

University of California  
Lawrence Berkeley Laboratory  
ATTN: Library, Bldg. 50, Rm. 134  
ATTN: Kenneth M. Watson

University of California  
Lawrence Livermore Laboratory  
ATTN: William J. Hogan, L-531  
ATTN: Frederick R. Kovar, L-94  
ATTN: Hans Kruger, L-96  
ATTN: Leland C. Loquist  
ATTN: Technical Information Department, L-3  
ATTN: Louis F. Wouters, L-24  
ATTN: Donald J. Meeker, L-153  
ATTN: Robert A. Anderson, L-156  
ATTN: Terry R. Donich

Los Alamos Scientific Laboratory  
ATTN: Document Control for John S. Malik  
ATTN: Document Control for J. Arthur Freed  
ATTN: Document Control for Richard L. Wakefield  
ATTN: Document Control for Reports Library  
ATTN: Document Control for J-8, R. E. Dartridge

Sandia Laboratories  
Livermore Laboratory  
ATTN: Document Control for Technical Library

Sandia Laboratories  
ATTN: Document Control for Charles N. Vittioe  
ATTN: Document Control for Elmer F. Hartman  
ATTN: Document Control for 5245, T. H. Martin  
ATTN: Document Control for Org. 9353, R. L. Parker  
ATTN: Document Control for Gerald W. Barr, 1114  
ATTN: Document Control for Org. 3141, Sandia Rpt. Coll.

U.S. Energy Research & Development Administration  
Albuquerque Operations Office  
ATTN: Document Control for WSSB  
ATTN: Document Control for Technical Library

Union Carbide Corporation  
Hollifield National Laboratory  
ATTN: Paul R. Barnes  
ATTN: Document Control for Technical Library

OTHER GOVERNMENT AGENCIES

Central Intelligence Agency  
ATTN: RD/SI for William A. Decker  
ATTN: RD/SI for Technical Library

Administrator  
Defense Electric Power Administration  
Department of the Interior  
ATTN: Document Control

Department of Commerce  
National Bureau of Standards  
ATTN: Technical Library

Department of Commerce  
National Oceanic & Atmospheric Administration  
ATTN: Classified Document Library

Federal Aviation Administration  
Headquarters Security Branch, ASE-210  
ATTN: ARD-350  
ATTN: Fredrick S. Sakate, ARD-350

NASA  
ATTN: Technical Library  
ATTN: Code Res. Guid. Con. & Info. Sys.

NASA  
Lewis Research Center  
ATTN: Library

DEPARTMENT OF DEFENSE CONTRACTORS

Aerojet Electro-Systems Co. Div.  
Aerojet-General Corporation  
ATTN: Technical Library  
ATTN: Thomas D. Hanscom

Aeronutronic Ford Corporation  
Aerospace & Communications Ops.  
ATTN: Fen C. Attinger  
ATTN: E. R. Poncelet, Jr.  
ATTN: L. B. Linder  
ATTN: Technical Information Section

Aeronutronic Ford Corporation  
Western Development Laboratories Division  
ATTN: Samuel R. Crawford, MS 531  
ATTN: J. T. Mattingly, MS X-22  
ATTN: Library

Aerospace Corporation  
ATTN: Bal Krishan  
ATTN: Melvin J. Bernstein  
ATTN: S. P. Bower  
ATTN: Julian Reinheimer  
ATTN: Irving M. Garfunkel  
ATTN: Dr. B. Barry  
ATTN: Norman D. Stockwell  
ATTN: Library

Avco Research & Systems Group  
ATTN: Research Library A830, Rm. 7201  
ATTN: W. Brodning

Battelle Memorial Institute  
ATTN: Technical Library  
ATTN: David A. Dingee  
ATTN: Dr. L. E. Hullbert

DEPARTMENT OF DEFENSE CONTRACTORS (Continued)

The BDM Corporation  
ATTN: Technical Library

The BDM Corporation  
ATTN: Technical Library  
ATTN: Robert B. Buchanan  
ATTN: T. H. Neighbors

Bell Aerospace Company  
Division of Textron, Inc.  
ATTN: Carl B. Schoch, Wpns. Effects Grp.  
ATTN: Martin A. Henry  
ATTN: Technical Library

The Bendix Corporation  
Communication Division  
ATTN: Document Control

The Bendix Corporation  
Research Laboratories Division  
ATTN: Technical Library  
ATTN: Donald J. Nichaus, Mgr. Prgm. Dev.

The Bendix Corporation  
Navigation & Control Division  
ATTN: Technical Library

The Boeing Company  
ATTN: David Kemle  
ATTN: David L. Dye, MS 87-75  
ATTN: Howard W. Wicklein, MS 17-11  
ATTN: D. E. Isbell  
ATTN: Dr. B. Lampriere  
ATTN: Aerospace Library

Booz-Allen & Hamilton, Inc.  
ATTN: Raymond J. Chrisner  
ATTN: Technical Library

Brown Engineering Company, Inc.  
ATTN: David L. Lambert, MS 18  
ATTN: John M. McSvain, MS 18  
ATTN: Technical Library, P. Shelton, MS 12

Burroughs Corporation  
Federal & Special Systems Group  
ATTN: Angelo J. Mauriello  
ATTN: Technical Library

Calspan Corporation  
ATTN: Technical Library

Charles Stark Draper Laboratory, Inc.  
ATTN: Technical Library  
ATTN: Kenneth Fertig

Cincinnati Electronics Corporation  
ATTN: Technical Library

Computer Sciences Corporation  
ATTN: Technical Library

Computer Sciences Corporation  
ATTN: Alvin T. Schiff

Cutler-Hammer, Inc.  
AIL Division  
ATTN: Anne Anthony, Central Technical Files

DEPARTMENT OF DEFENSE CONTRACTORS (Continued)

University of Denver  
Colorado Seminary  
ATTN: Security Officer for Ron W. Buchanan  
ATTN: Security Officer for Technical Library  
ATTN: Security Officer for Fred P. Venditti

The Dikewood Corporation  
ATTN: L. Wayne Davis  
ATTN: Technical Library

E-Systems, Inc.  
Greenville Division  
ATTN: Library 8-50100

Effects Technology, Inc.  
ATTN: Edward John Steele  
ATTN: B. Wengler  
ATTN: Technical Library

EG&G, Inc.  
Albuquerque Division  
ATTN: Technical Library

ESL, Inc.  
ATTN: Technical Library  
ATTN: William Metzger

Experimental & Mathematical Physics Consultants  
ATTN: Thomas M. Jordan

Fairchild Camera & Instrument Corporation  
ATTN: Security Department for Technical Library

Fairchild Industries, Inc.  
Sherman Fairchild Technology Center  
ATTN: Leonard J. Schreiber  
ATTN: Technical Library

The Franklin Institute  
ATTN: Ramie H. Thompson  
ATTN: Technical Library

Garrett Corporation  
ATTN: Technical Library

General Dynamics Corporation  
Pomona Operation  
ATTN: Technical Library

General Dynamics Corporation  
Electronics Division  
ATTN: Technical Library

General Electric Company  
Space Division  
ATTN: Technical Information Center  
ATTN: Larry I. Chasen  
ATTN: Joseph C. Peden, CCF-8301  
ATTN: Dante M. Tasca  
ATTN: James P. Spratt  
ATTN: Daniel Edelman  
ATTN: J. Hannabeck

General Electric Company  
Re-Entry & Environmental Systems Division  
ATTN: John W. Palehfsky, Jr.  
ATTN: Technical Library

DEPARTMENT OF DEFENSE CONTRACTORS (Continued)

General Electric Company  
Ordnance Systems  
ATTN: Joseph J. Reidl

General Electric Company  
TEMPO-Center for Advanced Studies  
ATTN: Royden R. Rutherford  
ATTN: DASIAC

General Electric Company  
ATTN: Richard C. Fries, CSP 6-7  
ATTN: Technical Library

General Electric Company  
Aircraft Engine Group  
ATTN: John A. Ellerhorst, E-2  
ATTN: Technical Library

General Electric Company  
Aerospace Electronics Systems  
ATTN: George Francis, Drop 233  
ATTN: Charles M. Howison, Drop 624  
ATTN: Technical Library

General Electric Company  
ATTN: Technical Library

General Research Corporation  
ATTN: John Ise, Jr.  
ATTN: Robert D. Hill  
ATTN: Technical Information Office

Grumman Aerospace Corporation  
ATTN: Jerry Rogers, Department 533  
ATTN: Technical Library

GTE Sylvania, Inc.  
Electronics Systems Group-Eastern Division  
ATTN: James A. Waldon  
ATTN: Charles A. Thornhill, Librarian  
ATTN: Leonard L. Blaisdell

GTE Sylvania, Inc.  
ATTN: Herbert A. Ullman  
ATTN: Mario A. Nurcfora, H & V Group  
ATTN: S. E. Perlman, A.S.M. Department  
ATTN: David P. Flood  
ATTN: Emil P. Motchok, Comm. Syst.

Harris Corporation  
Harris Semiconductor Division  
ATTN: Wayne E. Abare, MS 16-111  
ATTN: Carl F. Davis, MS 17-220  
ATTN: T. L. Clark, MS 4040  
ATTN: Technical Library

Hazeltine Corporation  
ATTN: M. Waite, Technical Information Center

Hercules, Incorporated  
ATTN: Technical Library  
ATTN: R. Woodruff, 100K-26-W

Honeywell Incorporated  
Government & Aeronautical Products Division  
ATTN: Ronald R. Johnson, A-1622  
ATTN: Technical Library

DEPARTMENT OF DEFENSE CONTRACTORS (Continued)

Honeywell Incorporated  
Aerospace Division  
ATTN: Stacey H. Graff, MS 725-J  
ATTN: Technical Library

Honeywell Incorporated  
Radiation Center  
ATTN: Technical Library

Hughes Aircraft Company  
ATTN: Billy W. Campbell, MS 6-E-110  
ATTN: Technical Library

Hughes Aircraft Company  
Ground Systems Group  
ATTN: Library, MS C-222

Hughes Aircraft Company  
Space Systems Division  
ATTN: Edward C. Smith, MS A-620  
ATTN: William W. Scott, MS A-1080  
ATTN: Technical Library

IBM Corporation  
ATTN: Frank Frankovsky  
ATTN: Technical Library

IIT Research Institute  
ATTN: ACOAT  
ATTN: Technical Library

IIT Research Institute  
ATTN: Irving N. Mindel  
ATTN: Technical Library

Institute for Defense Analyses  
ATTN: IDA Librarian, Ruth S. Smith

Intelcon: Rad Tech  
ATTN: R. L. Mertz  
ATTN: Ralph H. Stahl  
ATTN: Technical Library

International Telephone & Telegraph Corporation  
ATTN: J. Gulack, Def. Sp. Grp.  
ATTN: Technical Library

Ion Physics Corporation  
ATTN: Robert D. Evans  
ATTN: H. Milde  
ATTN: B. Evans  
ATTN: Technical Library

Johns Hopkins University  
Applied Physics Laboratory  
ATTN: Technical Library

Litton Systems, Inc.  
Data Systems Division  
ATTN: Technical Library

Litton Systems, Inc.  
Guidance & Control Systems Division  
ATTN: John P. Retzler  
ATTN: Val J. Ashby, MS 67  
ATTN: Technical Library

Ktech Corporation  
ATTN: Dr. D. Keller

DEPARTMENT OF DEFENSE CONTRACTORS (Continued)

Kaman Sciences Corporation  
ATTN: W. Foster Rich  
ATTN: Walter E. Ware  
ATTN: John R. Hoffman  
ATTN: Donald H. Bryce  
ATTN: Albert P. Bridges  
ATTN: Frank H. Shelton  
ATTN: T. Meagher  
ATTN: Dr. D. C. Sachs  
ATTN: J. C. Nickell  
ATTN: J. Oscarson  
ATTN: D. Williams  
ATTN: R. McClellan  
ATTN: E. Walsh  
ATTN: Dr. P. Wieselmann  
ATTN: Library

Litton Systems, Inc.  
AMECOM Division  
ATTN: Technical Library

Lockheed Missiles & Space Co. Inc.  
ATTN: George F. Heath, Dept. 81-14  
ATTN: Kevin McCarthy, 0-85-71  
ATTN: Hans L. Schneemann, Dept. 81-61  
ATTN: L-365, Dept. 81-20  
ATTN: Philip J. Hart, Dept. 81-14  
ATTN: Benjamin T. Kimura, Dept. 81-14  
ATTN: D. M. Tellep, Dept. 81-01  
ATTN: Dr. M. Miller  
ATTN: A. O. Burford  
ATTN: Technical Library

Lockheed Missiles & Space Company  
ATTN: P. G. Underwood  
ATTN: Technical Information Center, D/Coll.

LTV Aerospace Corporation  
Vought Systems Division  
ATTN: Technical Data Center

LTV Aerospace Corporation  
Michigan Division  
ATTN: James F. Sanson, B-2  
ATTN: Technical Library

M.I.T. Lincoln Laboratory  
ATTN: Leona Loughlin, Librarian A-082

Martin Marietta Aerospace  
Orlando Division  
ATTN: Mona C. Griffith, Lib., MP-30  
ATTN: Jack M. Ashford, MP-537

Martin Marietta Corporation  
Denver Division  
ATTN: Paul G. Kase, Mail 8203  
ATTN: Ben T. Graham, MS PO-454  
ATTN: Jay R. McKee, Research Library 6617

Maxwell Laboratories, Inc.  
ATTN: Richard A. Fitch  
ATTN: Victor Fargo  
ATTN: Technical Library

McDonnell Douglas Corporation  
ATTN: Tom Ender  
ATTN: Technical Library

DEPARTMENT OF DEFENSE CONTRACTORS (Continued)

McDonnell Douglas Corporation  
ATTN: W. R. Spark, MS 13-3  
ATTN: A. P. Venditt, MS 11-1  
ATTN: Stanley Schneider  
ATTN: Dr. R. J. Reck  
ATTN: Dr. H. M. Berkowitz  
ATTN: Technical Library Services

McDonnell Douglas Corporation  
ATTN: Thomas J. Lundregan

Mission Research Corporation  
ATTN: William C. Hart  
ATTN: Conrad L. Longmire  
ATTN: Daniel F. Higgins  
ATTN: Technical Library

Mission Research Corporation  
ATTN: David E. Merewether  
ATTN: Larry D. Scott  
ATTN: Technical Library

The Litre Corporation  
ATTN: Theodore Jarvis  
ATTN: Louis Brickmore  
ATTN: M. E. Fitzgerald  
ATTN: Library

National Academy of Sciences  
ATTN: R. S. Shane, Nat. Materials Advsy.

Northrop Corporation  
ATTN: George H. Towner  
ATTN: Vincent R. DeMartino  
ATTN: John M. Reynolds  
ATTN: Technical Library

Northrop Corporation  
ATTN: Technical Library

Northrop Corporation  
ATTN: Library  
ATTN: David M. Pocock

Palisades Inst. for Research Services Inc.  
ATTN: Records Supervisor

Perkin-Elmer Corporation  
ATTN: Technical Library

Philco-Aeronut  
ATTN: R. Lyons

Physics International Company  
ATTN: Document Control for Bernard H. Bernstein  
ATTN: Document Control for John H. Huntington  
ATTN: Document Control for Technical Library  
ATTN: Dr. J. Shea  
ATTN: K. Childers

Procedync Corporation  
ATTN: Peter Horowitz  
ATTN: Technical Library

Prototype Dev. Asso.  
ATTN: T. McKinley

R & D Assoc.  
ATTN: Dr. A. Field

DEPARTMENT OF DEFENSE CONTRACTORS (Continued)

R & D Associates  
ATTN: Gerard K. Schlegel  
ATTN: William R. Graham, Jr.  
ATTN: William J. Karzas  
ATTN: Charles Mo  
ATTN: Leonard Schlessinger  
ATTN: S. Clay Rogers  
ATTN: Robert A. Poll  
ATTN: Richard R. Schaefer  
ATTN: Technical Library

The Rand Corporation  
ATTN: Cullen Cram  
ATTN: Technical Library

Raytheon Company  
ATTN: Library  
ATTN: Cajanan H. Joshi, Radar Sys. Lab.

Raytheon Company  
ATTN: James R. Weckback  
ATTN: Technical Library

RCA Corporation  
Government & Commercial Systems  
ATTN: Technical Library

RCA Corporation  
Government & Commercial Systems  
ATTN: Andrew L. Warren  
ATTN: Technical Library

RCA Corporation  
Camden Complex  
ATTN: E. Van Keuren, 13-5-2  
ATTN: Technical Library

Rockwell International Corporation  
ATTN: K. F. Hull  
ATTN: Donald J. Stevens, FA-70  
ATTN: James E. Bell, HA-10  
ATTN: Technical Library

Rockwell International Corporation  
Space Division  
ATTN: TIC, D/41-092, AJ01

Rockwell International Corporation  
ATTN: T. B. Yates

Sanders Associates, Inc.  
ATTN: Moe L. Aitel, NCA 1-3236  
ATTN: Technical Library

Science Applications, Inc.  
ATTN: Frederick M. Tesche

Science Applications, Inc.  
ATTN: William L. Chadsey

Science Applications, Inc.  
ATTN: Lewis M. Linson  
ATTN: B. H. Fishbine  
ATTN: S. J. Dalich  
ATTN: J. N. Wood  
ATTN: R. Fisher  
ATTN: Technical Library

DEPARTMENT OF DEFENSE CONTRACTORS (Continued)

Science Applications, Inc.  
Huntsville Division  
ATTN: Noel R. Byrn  
ATTN: Technical Library

Science Applications, Inc.  
ATTN: James R. Hill  
ATTN: R. Parkinson  
ATTN: Richard L. Knight

Simulation Physics, Inc.  
ATTN: John R. Uglum

Simulation Physics, Inc.  
ATTN: R. Little

The Singer Company  
ATTN: Irwin Goldman, Eng. Management  
ATTN: Technical Library

Singer Information Systems Network  
ATTN: Technical Information Center

Southern Research Institute  
ATTN: C. Pears

Sperry Microwave Electronics Division  
Sperry Rand Corporation  
ATTN: Technical Library

Sperry Rand Corporation  
Univac Division  
Defense Systems Division  
ATTN: Technical Library

Sperry Rand Corporation  
Sperry Division  
Sci. Gyroscope Division  
ATTN: Paul Marraffino  
ATTN: Charles L. Craig, EV  
ATTN: Technical Library

Sperry Rand Corporation  
Sperry Flight Systems Division  
ATTN: D. J. Keating  
ATTN: Technical Library

Stanford Research Institute  
ATTN: Philip J. Dolan  
ATTN: William C. Taylor  
ATTN: Arthur Lee Whitson  
ATTN: George Carpenter  
ATTN: Dr. G. Abrahamson  
ATTN: SRI, Library, Rm. G-021

Stanford Research Institute  
ATTN: MacPherson Morgan  
ATTN: Technical Library

Sundstrand Corporation  
ATTN: Curtis B. White

Systems, Science & Software  
ATTN: Technical Library

Systems, Science & Software, Inc.  
ATTN: Dr. G. Gurtman

DEPARTMENT OF DEFENSE CONTRACTORS (Continued)

Systems, Science & Software, Inc.  
ATTN: Andrew R. Wilson  
ATTN: Technical Library

Systron-Donner Corporation  
ATTN: Technical Library

Texas Instruments, Inc.  
ATTN: Donald J. Manus, MS 72  
ATTN: Gary F. Hanson  
ATTN: Technical Library

TRW Semiconductors  
Division of TRW, Inc.  
ATTN: Technical Library

TRW Systems Group  
ATTN: William H. Robinette, Jr.  
ATTN: Fred N. Holmquist, MS R1-2028  
ATTN: Benjamin Sussholtz  
ATTN: Paul Molmud, R1-1196  
ATTN: Aaron H. Narevsky, R1-2144  
ATTN: A. M. Liebschutz, R1-1162  
ATTN: Lillian D. Singletary, R1-1070  
ATTN: Technical Information Center, S-1930  
ATTN: Robert M. Webb, MS R1-1150  
ATTN: Richard H. Kingsland, R1-2154  
ATTN: Dr. D. Jortner

TRW Systems Group  
San Bernardino Operations  
ATTN: John E. Dahnke  
ATTN: H. S. Jensen

DEPARTMENT OF DEFENSE CONTRACTORS (Continued)

TRW Systems Group  
8 cy ATTN: Technical Library

United Aircraft Corporation  
Hamilton Standard Division  
ATTN: Technical Library

United Technologies Corporation  
Norden Division  
ATTN: Technical Library

Victor A. J. Van Lint (Consultant)  
ATTN: V. A. J. Van Lint

Varian Associates  
ATTN: Howard R. Jory, A-109  
ATTN: Technical Library

Westinghouse Electric Corporation  
Astronuclear Laboratory  
ATTN: Technical Library

Westinghouse Electric Corporation  
Defense & Electronic Systems Center  
ATTN: Henry P. Kalapaca, MS 3525  
ATTN: Technical Library

Westinghouse Electric Corporation  
Research & Development Center  
ATTN: Technical Library

Official Record Copy/ Lt Mac Farlane, AFWL/DYV